ACS Chemical Neuroscience

Article

Discovery and Optimization of Chromone Derivatives as Novel Selective Phosphodiesterase 10 Inhibitors

Yan-Fa Yu, Chen Zhang, Yi-You Huang, Sirui Zhang, Qian Zhou, Xiangmin Li, Zengwei Lai, Zhe Li, Yuqi Gao, Yinuo Wu, Lei Guo, Deyan Wu, and Hai-Bin Luo

ACS Chem. Neurosci., **Just Accepted Manuscript** • DOI: 10.1021/acschemneuro.0c00024 • Publication Date (Web): 27 Feb 2020

is published by the American Chemical Society. 1155 Sixteenth Street N.W., Washington, DC 20036

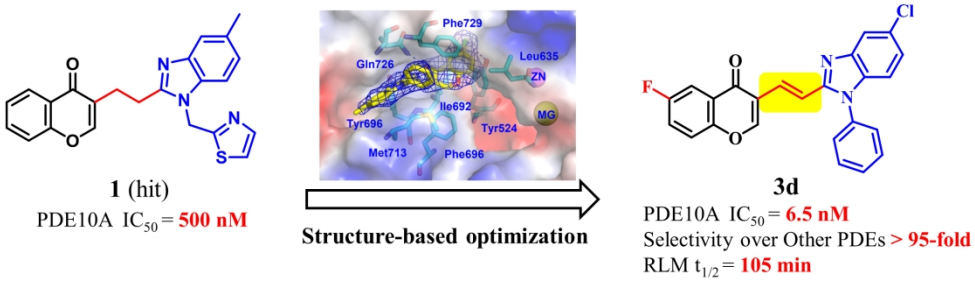

199x60mm (300 x 300 DPI)

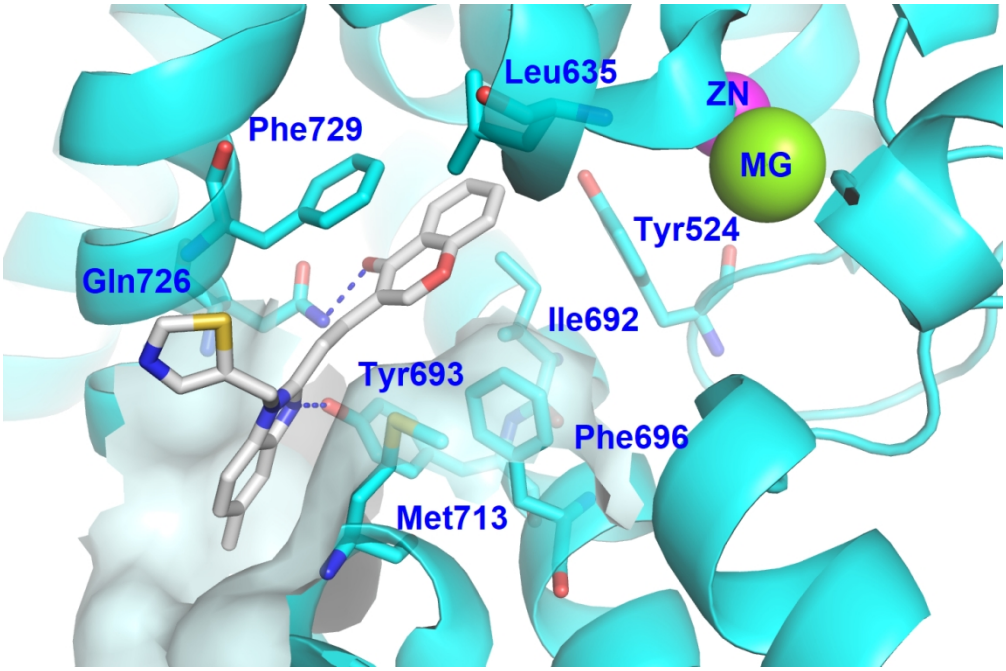

386x256mm (96 x 96 DPI)

Discovery and Optimization of Chromone Derivatives as Novel Selective Phosphodiesterase 10 Inhibitors

Yan-Fa Yu[||], Chen Zhang[||], Yi-You Huang[||], Sirui Zhang, Qian Zhou, Xiangmin Li, Zengwei Lai, Zhe Li, Yuqi Gao, Yinuo Wu, Lei Guo*, Deyan Wu*, and Hai-Bin Luo

School of Pharmaceutical Sciences, Sun Yat-sen University, Guangzhou 510006, China

ABSTRACT

Phosphodiesterase 10 (PDE10) inhibitors have received much attention as promising therapeutic agents for central nervous system (CNS) disorders such as schizophrenia and Huntington's disease. Recently, a hit compound **1** with a novel chromone scaffold has showed moderate inhibitory activity against PDE10A (IC_{50} = 500 nM). Hit-to-lead optimization has resulted in compound **3e** with an improved inhibitory activity (IC_{50} of 6.5 nM), remarkable selectivity (> 95-fold over other PDEs), and good metabolic stability (RLM $t_{1/2}$ = 105 min) by using an integrated strategy (molecular modeling, chemical synthesis, bioassay, and cocrystal structure). The cocrystal structural information provides insights into the binding pattern of **3e** in the PDE10A catalytic domain to highlight the key role of the halogen and hydrogen bonds toward Tyr524 and Tyr693, respectively, thereby resulting in high selectivity against other PDEs. These new observations are of benefit for the rational design of the next generation PDE10 inhibitors for CNS disorders.

Keywords: Phosphodiesterase 10A, chromone derivatives, cocrystal structure, metabolic stability, molecular docking, schizophrenia

INTRODUCTION

Schizophrenia is a common psychiatric illness characterized by basic personality changes, thinking, emotion and behavior splitting, mental activities, and environmental disharmony.[1] Schizophrenia affects ~ 0.7 % of the world's population, especially affecting a large number of young adults with lifelong social and communication disorders.[2] Currently, the pathophysiology of schizophrenia has not yet been fully elucidated meanwhile schizophrenia can be roughly characterized by positive

(delusions, hallucinations, thinking and behavior disorder), negative (emotional apathy, social dysfunction and lack of motivation) and cognitive (impairment of action, attention, learning and memory) symptoms.[3] Although typical and atypical antipsychotic drugs, including chlorpromazine, olanzapine and risperidone, show curative effect on positive psychotic symptoms by means of modulating dopamine 2 (D2) and 5-HT receptors, they are less effective in alleviating negative symptoms and cognitive disorders. Furthermore, most current antipsychotic agents have non-ignorable adverse effects, including extrapyramidal syndrome (such as acute dystonia), vegetative system dysfunction (such as xerostomia and postural hypotension), weight gain and hyperprolactinemia.[4-6] Up to now, the medical needs for treatment of schizophrenia is unmet, especially for a definite curative effect on negative symptoms and cognitive symptoms as well as treatment resistance. Therefore, discovery and development of new drugs targeting novel targets for schizophrenia is still an urgent demand.[7]

Phosphodiesterases (PDEs) as a superenzyme family (PDE 1~ 11) are in charge of hydrolyzing the ubiquitous secondary messengers adenosine 3',5'-cyclic monophosphate (cAMP) to 5'-AMP and guanosine 3',5'-cyclic monophosphate (cGMP) to 5'-GMP, respectively.[8] Inhibition of PDEs can prolong or enhance the effects of physiological processes mediated by cAMP and/or cGMP, and has proved to be therapeutic for various diseases,[9-11] such as PDE5 inhibitor sildenafil for erectile dysfunction and pulmonary arterial hypertension (PAH).[12, 13] It has been reported that abnormalities in cAMP signalling pathways was responsible for the pathophysiology of symptoms in schizophrenia.[14, 15] In addition, cGMP might be involved in the pathophysiology of cognitive symptoms in schizophrenia, since it related to short-term changes in excitability in striatal neurons.[16]

Phosphodiesterase 10 (PDE10), a dual-substrate enzyme hydrolyzing both cAMP and cGMP, is highly expressed in the medium spiny neurons of the striatum (MSNs) in central nervous system (CNS) of many mammalian species.[17] It is thought to be a promising drug target for CNS disorders such as schizophrenia and Huntington's disease.[18-20] PDE10 knockout mice were observed with reduced hyperactivity response

in the locomotor activity model, which were likely triggered to have schizophrenic-like behaviors by phencyclidine.[21] Phosphodiesterase 10A (PDE10A) inhibitors are expected to modulate via cAMP- and cGMP-dependent mechanisms both the dopamine D1-direct and D2-indirect striatal pathways and regulate the phosphorylation status of a panel of glutamate receptor subunits in the striatum.[7] Papaverine, a commercial drug capable of inhibiting PDE10, was prior reported to exhibit curative effect in rat models of schizophrenia.[21, 22] During the last two decades, an increasing number of patents on novel PDE10 inhibitors have been applied by pharmaceutical companies, but few results of clinical trials on the possibility of using PDE10 inhibitors as drug candidates for schizophrenia or Huntington's disease have been published (**Figure 1**).[23-28] Despite the promising safety profile of MP-10 exploited by Pfizer, clinical trials were terminated at Phase II (NCT01939548) due to dissatisfactory pre-specified criteria for efficacy (NCT01939548) as well as schizophrenic patients suffering an acute exacerbation of symptoms (NCT01175135). Recently, a clinical Phase II study of the effects of PDE10 inhibitor TAK-063 on the primary and secondary endpoints may be suggestive of antipsychotic activity, but the higher risk of extrapyramidal syndromes has also been found in contrast with the placebo group.[29] Only OMS824 from Omeros pipeline has received the designation of Orphan Drug for treating Huntington's disease as well as the designation of Fast Track drug for treating cognitive impairment observed in patients suffering from Huntington's disease, but the results are yet to be published.[25] These clinical trial results highlight that PDE10 inhibitors are still urgently expected to be developed to improve CNS disorder outcomes with reduced adverse effects.

A pre-screening of our internal compound library for novel PDE10 inhibitors identified compound **1** (**Figure 2**) with a novel chromone scaffold, which had never been reported among PDE10 inhibitors. As compound **1** only showed modest inhibitory activity against PDE10 with an IC_{50} value of 500 nM, further structural optimizations with the aid of cocrystal structure and molecular modeling were performed to find compound **3e** with remarkably improved inhibitory activity (IC_{50} = 6.5 nM) and metabolic stability (RLM $t_{1/2}$ of 105 min).

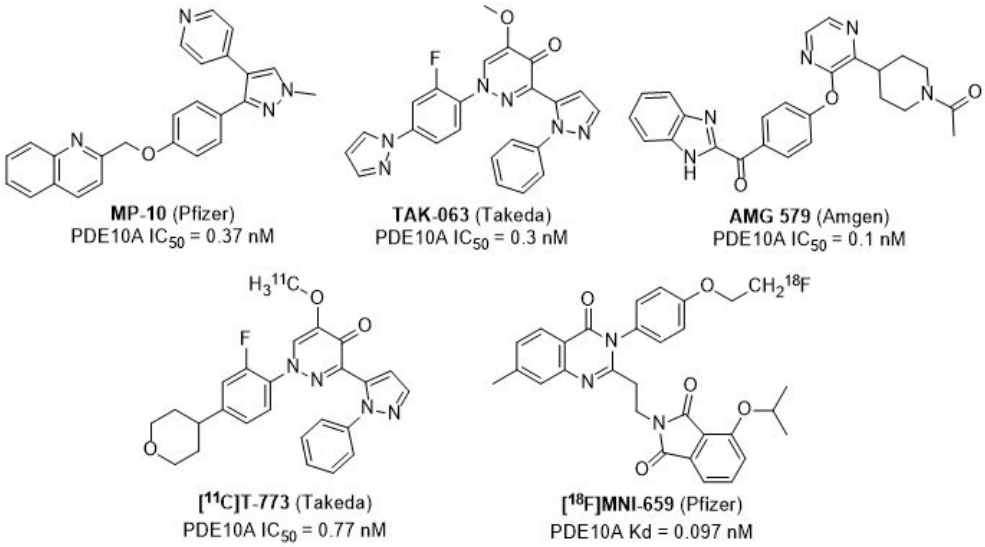

Figure 1. Structure of PDE10A inhibitors in clinical trials.

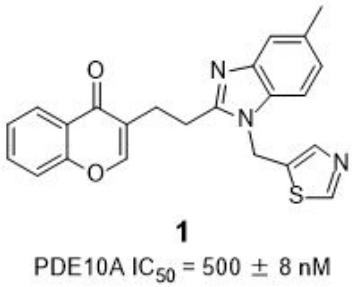

Figure 2. Structure of hit compound **1**.

RESULTS AND DISCUSSION

Rational Structural Design Based on the Binding Mode of Compound 1 with PDE10A

Molecular docking and molecular dynamics (MD) simulations were performed to investigate the possible binding pattern between compound **1** and PDE10A. As shown in **Figure 3**, the chromone scaffold of **1** formed a hydrogen bond with the conserved Gln726 and π–π stacking interaction with the hydrophobic clamp contributed by Phe729 and Ile692/Phe696, which were two characteristic interactions conserved in all PDE inhibitors.[30] Additionally, the ethyl linker stretched towards the unique selectivity pocket (Q2 pocket), which provided an optimal access for the thiazol-5-ylmetyl benzimidazole motif of **1** to be inserted into and an available H-bond formed with Tyr693.

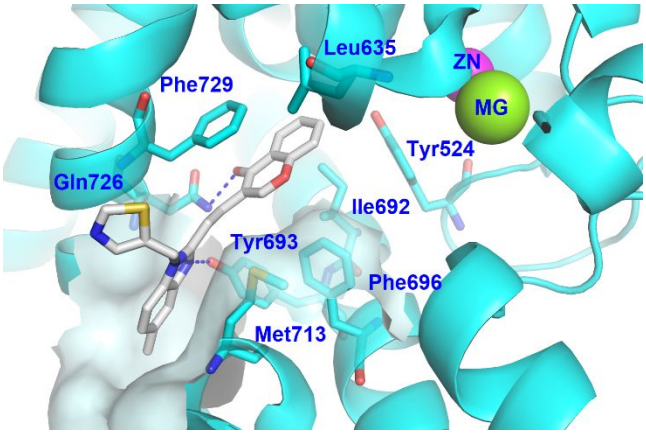

Figure 3. The predicted binding mode of the hit compound **1** with PDE10A.

As is known, most potent and selective PDE10A inhibitors were reported to interact with this unique selectivity Q2 pocket.[31, 32] Therefore, different substituents on the benzimidazole moiety of **1** were firstly designed to obtain more appropriate binding groups toward Q2 pocket. The chromone scaffold of **1** was retained to keep the representative interactions with conserved Gln726 and Phe729. Prior to chemical synthesis, the binding modes of designed compounds with PDE10A were predicted by molecular docking and dynamics simulations, and the binding free energies were estimated by MM-GBSA method. In addition, the root mean square deviation (RMSD) plots and hydrogen/halogen bond analysis for each system during MD simulations are shown in **Figure S1, S2** and **S3** in Supporting Information.[33, 34] According to the computational results, potential compounds were selected for synthesis and biological evaluation. The structure-activity relationship (SAR) results are summarized in **Table 1**.

Table 1. The inhibitory activity of compounds **1a-1k** against PDE10A and their estimated binding free energies.

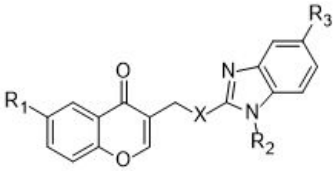

Cp.	R_1	R_2	R_3	X	IC_{50} (nM)[a]	GBTOT (kcal/mol)[b]
1a	H	H	CH_3	S	>1000	-29.07±2.86
1b	H	H	CH_3	S=O	>1000	-29.49±2.29
1c	Cl	H	CH_3	C	112 ± 8	-36.01±2.30

1d	H	H	OCH_3	C	>100	-33.72±2.36
1e	H	H	CF_3	C	>100	-32.73±2.54
1f	H		CH_3	C	355 ± 16	-39.77±2.23
1g	H	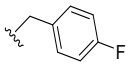	CH_3	C	>100	-39.04±2.88
1h	H	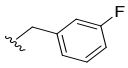	CH_3	C	>100	-38.95±4.06
1i	H		CH_3	C	52 ± 3	-38.47±3.18
1j	H		CH_3	C	76 ± 6	-38.45±2.76
1k	H		Cl	C	95 ± 11	-38.70±3.02

[a] Values are means of three independent experiments.

[b] Binding free energies are relative values estimated by MM-GBSA method.

The First-round of Optimization Assisted with MD Simulations to Result in 1i with Inhibitory Potency Increased by 10-Fold

The hit compound **1** could be roughly divided into three major parts, including a chromone scaffold, an ethyl linker and a substituted benzimidazole moiety (selective pocket binding group, SPBG). Firstly, while the substitution at the *N*-1 position of SPBG was absent, the key ethyl linker replaced simply by a thioethyl or sulfoxide ethyl group afforded **1a** or **1b** with a remarkable lost in PDE10A inhibitory activity. Comparing with **1a** or **1b**, compound **1c** based on the ethyl linker had a simple -Cl substituent at the 6-position of the chromone scaffold to surprisingly exhibit increasing inhibition with an IC_{50} value of ~112 nM, indicating the ethyl linker as a crucial fragment for inhibitory potency. Remarkable increases of ~7 kcal/mol in the absolute values of predicted binding free energies (MM-GBSA total energy, GBTOT) from **1a** and **1b** to **1c** were also observed, further convincing that the ethyl group rather than the thioethyl or sulfoxide ethyl group was favorable to binding Q2 pocket. However, -OCH_3 or -CF_3 substituent replacing the -CH_3 group at the 5-position of the benzimidazole fragment was investigated to obtain **1d** or **1e** with no enhancement in potency, which was in consistence with the predicted binding free energy values. Given that trifluoromethyl and the methyl groups were comparable in size, the

decreased affinity of **1e** might be attributed to the unfavorable electrostatic repulsions while **1d** with a methoxy group could provide steric hindrance toward the narrow space of Q2 pocket. As the methyl group fixed at the 5-position of benzimidazole, various substituents at the *N*-1 position of benzimidazole were designed to tune the inhibitory potency such as benzyl, fluorobenzyl, phenyl and pyridyl groups. Binding patterns and affinities for **1f-1k** with PDE10 were pre-estimated by molecular docking and MD simulations. All these compounds were predicted to possess better binding affinities with an increase in the absolute values of GBTOT from 2.4 to 3.7 kcal/mol, which suggested that aromatic rings at 5-position might benefit for binding. As depicted in **Table 1**, compounds with benzyl (**1f**) or fluorobenzyl (**1g**, **1h**) group at the *N*-1 position showed slightly improved inhibitory activity while compounds with phenyl (**1i**, **1k**) or pyridyl ring (**1j**) exhibited a great enhancement of inhibitory potency. It was worth mentioning that **1i** owning 5-methyl-1-pheyl benzimidazole group showed a 10-fold enhancement in inhibitory activity (IC_{50} = 52 nM) comparing with **1**. However, the 4-pyridyl ring on SPBG instead of the phenyl ring could give rise to a slight decrease of inhibitory activity. The SAR study indicated that the phenyl ring was a preferable substituent at the *N*-1 position of benzimidazole, which fitted the selective pocket of PDE10 better.

The synthetic route of benzimidazole derivatives **1a-1b** is outlined in **Scheme 1**. 3-(hydroxymethyl)-4*H*-chromen-4-one **3** was synthesized from commercially available 4-oxo-4*H*-chromene-3-carbaldehyde **2**. [35] Brominating of **3** with CBr_4 gave **4**. Compound **4** was reacted with 5-methyl-1,3-dihydro-2*H*-benzo[*d*]imidazole-2-thione to obtain **1a**, which was oxidized by Oxone to afford compound **1b**.[36,37]

The synthetic route of **7a-7i** is outlined in **Scheme 2**. A Buchwald–Hartwig reaction of **8** with corresponding aryl amine gave the nitro aniline analogues **10a-10e**.[38] Catalytic hydrogenation of **10a-10e** yielded the phenylenediamines **7d-7h.** On the other hand, a reaction of the **11** with an excess of aniline gave the nitro aniline derivative **13**. The compound **13** was treated under catalytic hydrogenation conditions to give **7i**.

The synthesis of benzimidazole analogues **1c-1k** is shown in **Scheme 3**. One pot reaction of **2** or **5** with cyclic malonate in the presence of triethylamine and formic acid

(1:1) under reflux for 2 h gave carboxylic acid **6a-6b**.[39] Compound **6a** or **6b** was condensed with the phenylenediamine derivative **7a-7i** in the presence of HATU and DIPEA and then cyclized in acetic acid to give **1c-1k**.[40]

Scheme 1. General procedures used to synthesize compounds **1a-1b.**

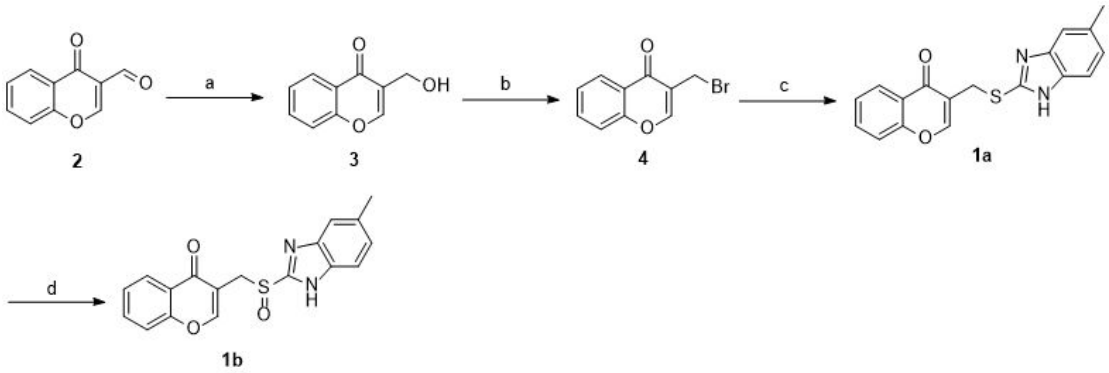

Reagents and conditions: (a) Al_2O_3, isopropyl alcohol, 75 °C, 4 h; (b) CBr_4, PPh_3, CH_2Cl_2, rt, 4 h; (c) Et_3N, DMF, 80 °C, 12h; (d) Oxone, ethyl acetate, rt, 1h.

Scheme 2. General procedures used to synthesize compounds **7a-7i**.

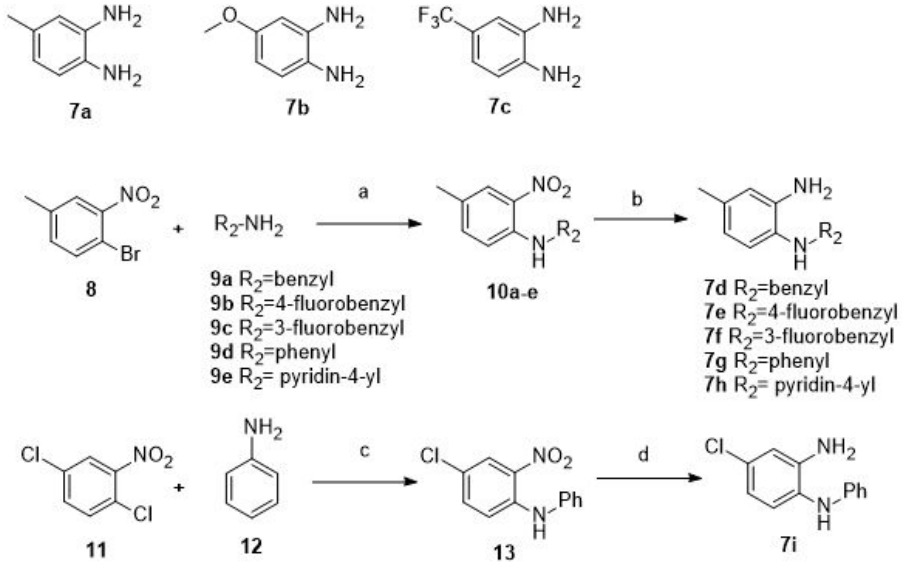

Reagents and conditions: (a) $Pd_2(dba)_3$, PhMe, Cs_2CO_3, BINAP, 110 °C, 24 h; (b) H_2, $Pd(OH)_2/C$, EtOH, rt, 6 h or $SnCl_2$, ethyl acetate, reflux, 2 h; (c) K_2CO_3, DMSO, 120 °C, 12h; (d) $SnCl_2$, ethyl acetate, reflux, 2 h.

Scheme 3. General procedures used to synthesize compounds **1c-1k.**

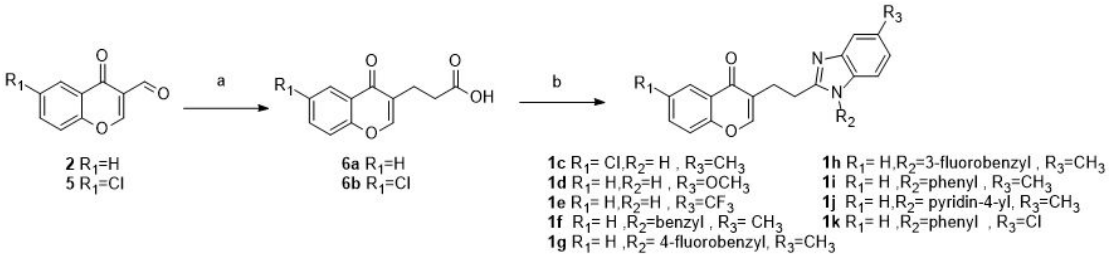

Reagents and conditions: (a) Cyclic malonate, Et_3N, HCO_2H, reflux, 2-3 h; (b) i) **7a-7i**, HATU, DIPEA, CH_2Cl_2, rt, 12 h; ii) Acetic acid, 90 ^oC,12 h.

Halogen Bonds were Important to Increase Inhibitory Potency Illustrated by Cocrystal Structures

To validate the binding modes between the chromone inhibitors and PDE10A, the cocrystal structure of compound **1i** with PDE10A was successfully determined (PDB ID: 6KO0). As shown in **Figure 4A**, the electron density in (2Fo-Fc) and (Fo-Fc) unambiguously showed that **1i** bound to the catalytic pocket of PDE10A. The chromone moiety of **1i** served as the scaffold to be sandwiched in the hydrophobic clamp between Phe729 and Phe696/Ile692, while the carbonyl oxygen provided a strong H-bond with the amide nitrogen of conserved Gln726. Furthermore, the 5-methyl-1-phenyl benzimidazole group of **1i** was fitted well into the Q2 pocket meanwhile an H-bond between the 3-N of the benzimidazole group and Tyr693 was also observed. Notably, the binding mode revealed by cocrystal structure was consistent with the predicted pattern derived from MD simulations (**Figure 4B**), illustrating that the MD-based protocol employed in the present study was reliable.

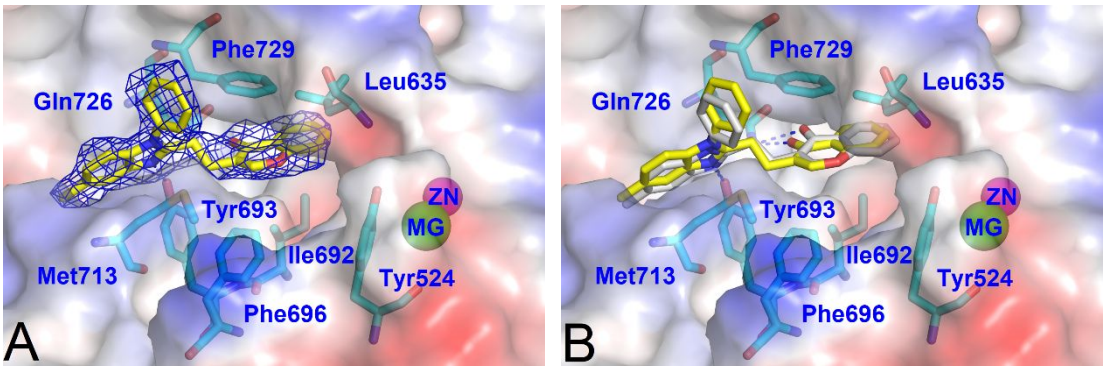

Figure 4. (A) Cocrystal structure of PDE10-**1i** (PDB ID: 6KO0). The 2Fo-Fc electron density is contoured in dark blue at 1.0 σ. (B) Alignment of the crystal structure (yellow) and the predicted structure (off-white) of PDE10-**1i**.

The cocrystal structure of PDE10A with **1i** implied that further optimization could be implemented in several sites. Recently, halogen bonding, noncovalent intermolecular interaction occurring between Lewis bases (O, N, and S) and Lewis acids (Cl, Br, and I), had been recognized as a prevalent ligand-protein interaction, which were successfully utilized to improve the potency of PDE5 inhibitors.[41] In our case of PDE10-**1i**, the C-6 position of the chromone ring seemed to be an appropriate site for halogenation since it was close to the phenolic hydroxyl group of Tyr524 with a distance of 3.8 Å. Small halogen substituents at the C-6 position of chromone were expected to be well-tolerated and to build up a potential interaction with Tyr524 by means of halogen bond. Thus, halogen substituents (F, Cl, Br and I) were introduced at the C-6 position of the chromone moiety to afford compounds **2a**, **2b**, **2c** and **2d**, respectively. Prior to synthetic and bioassay work, binding free energies were also calculated based on the predicted binding poses of **2a**, **2b** and **2d** with PDE10. As supposed, halogen bonds were observed for each compound binding PDE10 in docking patterns and MD trajectories. In addition, 0.7~2.5 kcal/mol increase in the absolute values of GBTOT from **1i** to **2a**, **2b** and **2d** indicated that halogenation was applicable. As a result, distinct improvement of inhibitory potency through these simple modifications was inspiring. As depicted in **Table 2**, fluoro- (**2a)**, chloro- (**2b)** and bromo- (**2c)** substituted derivatives exhibited increased inhibitory activity against PDE10A by about 2-3 times referring to **1i** except iodine analogue **2d**, indicating that the relatively big radius of the iodine atom was detrimental to form halogen bond with Tyr524. Similarly, introducing 6-methoxy group to the chromone afforded **2e** with potency enhanced by about 3-fold, which might be on account of an extra hydrogen bond associated with Tyr524.

Table 2. The inhibitory activities of compounds **2a-2e** against PDE10A and their estimated binding free energies.

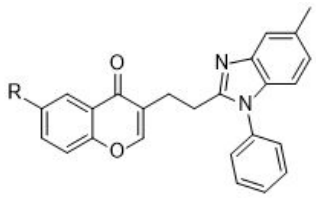

Cp.	R	IC_{50} (nM)[a]	GBTOT (kcal/mol)[b]
2a	F	17 ± 1	-39.55±2.76
2b	Cl	22 ± 2	-39.16±2.44
2c	Br	34 ± 2	-40.94±3.78
2d	I	54 ± 5	nd[c]
2e	OCH_3	18 ± 2	-39.65±3.01

[a] Values are means of three independent experiments.

[b] Binding free energies are relative values estimated by MM-GBSA method.

[c] Not determined.

The cocrystal structure of **2b** bound in PDE10A (PDB ID: 6KO1) was also successfully determined. As shown in **Figure 5**, **2b** primarily interacted with Gln726 and Phe729 of PDE10A via a hydrogen bond and π–π stacking, respectively, besides a hydrogen bond with Tyr693 in the Q2 pocket. These interactions were similar to that of **1i**. Interestingly, an extra halogen bond was formed between chlorine atom of **2b** and Tyr524, which contributed to the enhancement of inhibitory activity against PDE10A. The synthesis of benzimidazole analogues **2a-2e** are shown in **Scheme 4**. Initially, one pot reaction of **5**, **14a-14d** and cyclic malonate in the presence of triethylamine and formic acid (1:1) under reflux for 2 h gave carboxylic acid **15a-15e**. Compound **15a-15e** were condensed with the phenylenediamine derivative **7g** in the presence of HATU and DIPEA and then cyclized in acetic acid to give **2a-2e**.

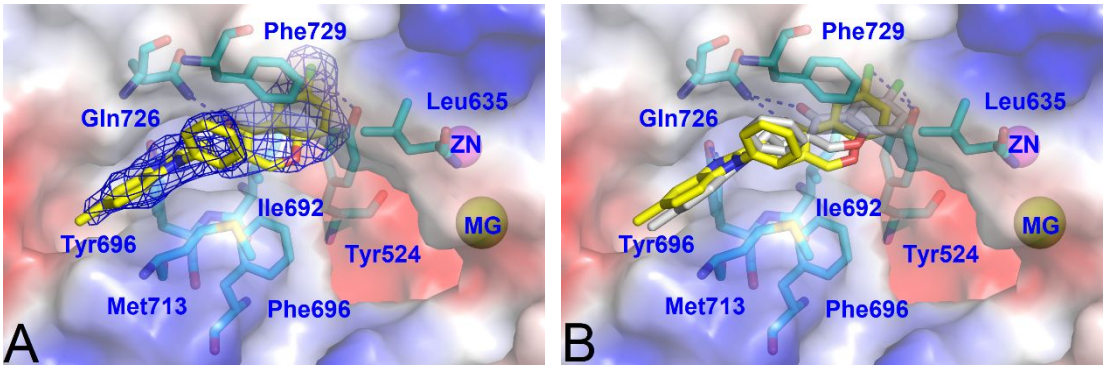

Figure 5. (A) Cocrystal structure of PDE10-**2b** (PDB ID: 6KO1). The 2Fo-Fc electron density is contoured in dark blue at 1.0 σ. (B) Alignment of the crystal structure (yellow) and the predicted structure of PDE10-**2b** (off-white).

Scheme 4. General procedures used to synthesize compounds **2a-2e**.

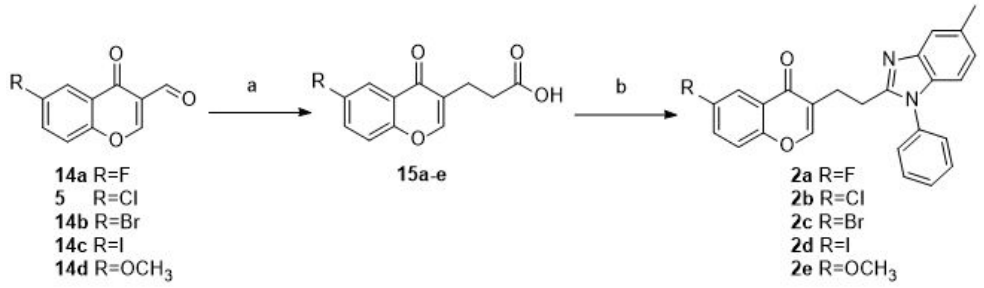

Reagents and conditions: (a) Cyclic malonate, Et_3N, HCO_2H, reflux, 2-3 h; (b) i) **7g**, HATU, DIPEA, CH_2Cl_2, rt, 12 h; ii) Acetic acid, 90 ^oC, 12 h.

The Third-round of Optimization Resulted in a Nanomolar and Metabolically Stable PDE10A Inhibitor

Although the structure-based optimizations from the hit compound **1** to **2b** were effective and inspiring assisted with molecular docking and MD simulations, high *in vitro* clearance of **2b** was also observed with half-life ($t_{1/2}$) of 0.58 min in rat liver microsomes (RLM) test, which was detrimental for further *in vivo* study. To improve the metabolic stability and pharmacokinetic properties of **2b**, the third-round optimization was performed in the possible metabolic sites on the chromone scaffold as well as the ethyl linker.

Molecular docking suggested that the benzimidazole group of **2b** could also stretched to the unique selective pocket by replacing the ethyl linker with vinyl one. Molecular docking and MD simulations confirmed that introducing the vinyl linker for newly designed compounds didn't cause major alternations in binding patterns and in binding affinities compared with **2b**. The predicted binding free energies (GBTOT) for **3a-3f** with PDE10 ranged from -38.10 to -40.16 kcal/mol, which well matches **2i** with 39.16 kcal/mol. Compound **3a** was designed with a vinyl linker and found to be improved in both metabolic stability (RLM $t_{1/2}$ of 8.68 min) and inhibitory potency (IC_{50} of 7.9 nM). The introduction of a nitrogen atom at the 7-position of the benzimidazole ring was successful to afford **3b** with less inhibitory activity than **3a**. Besides, the metabolic stability of compound **3c** with chlorine atom at 5-position of the benzimidazole ring was further improved with RLM $t_{1/2}$ of 13.0 min. Compound **3d** regarded as a vinyl analogue of **2b**, exhibited both good inhibitory activity (IC_{50} = 7.7 nM) and good metabolic stability with RLM $t_{1/2}$ of 23.3 min, thereby corroborating the

C=C bond linker enhancing the metabolic stability meanwhile the chlorine atom at 5-position of the benzimidazole ring was benefit for preventing the compound from metabolic degradation. In other words, the ethyl linker and the methyl group at the 5-position of the benzimidazole ring of **2b** seemed to be simultaneously prone to the metabolic degradation. (**Table 3**). The cocrystal structure of PDE10A with **2b** implied that a halogen bond was formed between the chromone scaffold and Tyr524, we speculated that the C-6 position of chromone scaffold was a probable metabolic site. It was a deliberate attempt to introduce the fluorine atom at C-6 position of the chromone scaffold to obtain **3e** with a slight improvement on PDE10A inhibitory potency (IC_{50} = 6.5 nM). More importantly, **3e** had a dramatic improvement on metabolic stability with RLM $t_{1/2}$ of 105 min. Conversion of monochloro-substituted **3c** to dichloro-substituted **3f**, in spite of significant enhancement in metabolic stability, led to a significant loss of inhibitory activity on account of the disruption of the H-bond interaction between **3f** and Gln726 as well as extremely poor solubility. Although the clinical candidate TAK-063 exhibited more advantages of inhibitory activity and metabolic stability, compound **3e** also indicated desirable properties as a potential PDE10 inhibitor. Our findings suggest that C-6 position of the chromone scaffold is a probable metabolic site in this series of PDE10 inhibitors.

Table 3. The inhibitory activities of compounds **3a-3f** and **TAK-063** against PDE10A，their estimated binding free energies, and rat microsomal stability.

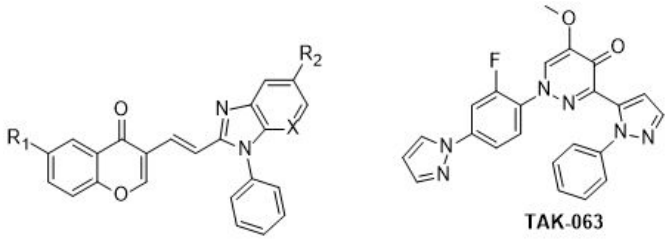

Cp.	R_1	X	R_2	IC_{50} (nM)[a]	GBTOT (kcal/mol)[b]	RLM $t_{1/2}$ (min)[c]
3a	H	C	CH_3	7.9±0.4	-39.19±2.53	8.68
3b	H	N	CH_3	22 ± 4.0	-38.36±2.20	nd[d]
3c	H	C	Cl	11 ± 1.7	-38.10±2.40	13.0
3d	Cl	C	CH_3	7.7 ± 0.7	-40.16±2.71	23.3
3e	F	C	Cl	6.5 ± 0.4	-39.70±2.61	105
3f	Cl	C	Cl	>100	-39.32±2.22	336

TAK-063	0.30 ± 0.10	213

[a] Values are means of three independent experiments.

[b] Binding free energies are relative values estimated by MM-GBSA method.

[c] $t_{1/2}$, calculated *in vitro* elimination half-life

[d]Not determined.

The binding mode of **3e** with PDE10A was predicted by molecular modeling as illustrated in **Figure 6**. Ideally, the vinyl linker together with the benzimidazole group well matched the narrow Q2 pocket and bonded to the chromone scaffold in the hydrophobic clamp consisting of Phe729 and Phe696/Ile692. Notably, both hydrogen bond with Gln726/Tyr693 and the halogen bond with Tyr524 were obviously pointed out to make sense out of good inhibitory potency. Benzimidazole analogues **3a-3f** were prepared according to the synthesis route in **Scheme 5**. The carboxylic acid **16a-16c** were obtained from a Knoevenagel-Doebner condensation.[42] Compound **16a-16c** were condensed with the phenylenediamine derivative **7g** or **7i** in the presence of HATU and DIPEA and then cyclized in acetic acid to give **3a-3f**.

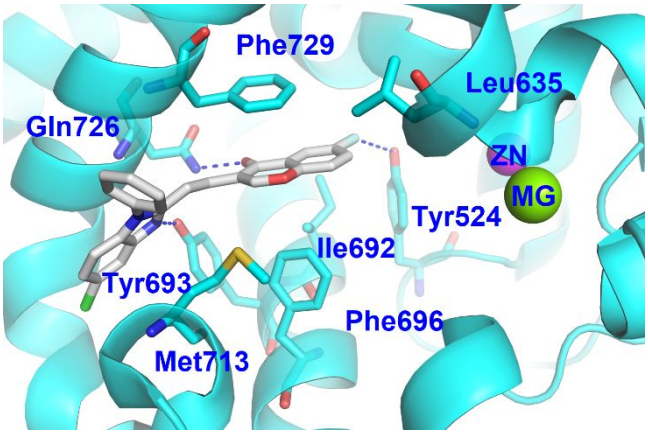

Figure 6. The predicted binding mode of compound **3e** with PDE10A.

Scheme 5. General procedures used to synthesize compounds **3a-3f.**

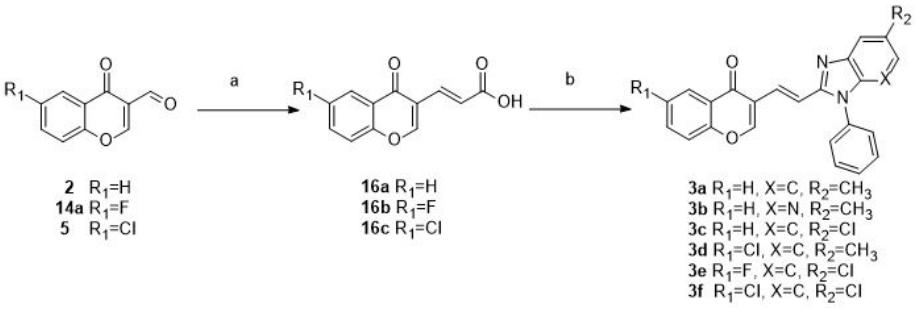

Reagents and conditions: (a) pyridine, malonic acid, reflux, 45 min; (b) i) **7g** or **7i**, HATU, DIPEA, CH_2Cl_2, rt, 12 h; ii) Acetic acid, 90 ^oC, 12 h.

Remarkable Selectivity of 3e Against other PDE Isoforms.

Compound **3e** with the good affinity and desirable metabolic stability was also evaluated for the selectivity across other PDE isoforms. As shown in **Table 4**, **3e** revealed ideal PDE10 selectivity more than 100-fold over PDE1B, 2A, 3A, 4D, 7A, 8A, and 9A except PDE5A. However, the IC_{50} value of **3e** against PDE5A was still determined as ~620 nM, corresponding to 95-fold selectivity. These results demonstrate that **3e** is a potent and highly selective PDE10A inhibitor, which has the potential to be exploited for further pharmacological research in the future.

Table 4. Selectivity of compound **3e** toward PDEs isoforms.

PDEs	IC_{50} (μM)	Selectivity
PDE10A2(449-770)	0.0065 ± 0.0004	-
PDE1B(10-487)	> 10	>1524-fold
PDE2A(580-919)	2.82 ± 0.43	430-fold
PDE3A(679-1087)	>10	>1524-fold
PDE4D2(86-413)	0.86 ± 0.21	131-fold
PDE5A1(535-860)	0.62 ± 0.03	95-fold
PDE7A1(130-482)	> 10	>1524-fold
PDE8A1(480-820)	3.40 ± 0.67	518-fold
PDE9A2(181-506)	2.08 ± 0.38	317-fold

CONCLUSION

In summary, pre-screening of our internal compound library discovered a novel chromone-scaffold hit compound **1** with modest PDE10 inhibitory activity (IC_{50} = 500 nM). Three rounds of structural optimization were performed with the aid of cocrystal structure, molecular docking and MD simulations. In particular, the satisfying strategy for the structural optimization was performed to prevent this series of the chromone compounds from the metabolic degradation *via* two available approaches. One is the rigid vinyl linker instead of the rotatable ethyl linker. Another is that halogen atom is suitable to be introduced on the chromone scaffold and the benzimidazole group, indicating the possible metabolic site on the base of this molecular skeleton. This efficient strategy for novel structural discovery resulted in 13 compounds with IC_{50}

values ranging from 1 to 100 nM and 3 compounds with an IC_{50} value less than 10 nM. The lead compound **3e** exhibited sufficient inhibitory activity against PDE10A (IC_{50} = 6.5 nM), remarkable selectivity against other PDEs (> 95- fold) and desirable metabolic stability (RLM $t_{1/2}$ of 105 min). Our study presents an excellent example for efficient structural optimization of novel PDE10 inhibitors for the potential CNS drug discovery.

METHODS

Chemistry

Unless specified, all reagents and starting materials were purchased from commercial sources and used as received. Analytical thin layer chromatography (TLC) was performed using pre-coated silica gel plate. Visualization was achieved by UV light (254 nm). Column chromatography was performed using silica gel. ^{1}H NMR and ^{13}C NMR spectra were recorded on a BrukerBioSpin GmbH spectrometer at 400.1 and 100.6 MHz, respectively. Coupling constants are given in Hz using TMS as an internal standard and $CDCl_3$ or DMSO - d_6 or MeOD as solvents. Chemical shift is given in ppm (δ). High-resolution mass spectra (HRMS) were obtained on an IT-TOF mass spectrometer. The purity of the compounds was determined by reverse-phase high-performance liquid chromatography (HPLC) analysis and confirmed to be more than 95%. HPLC instrument: SHIMADZU LC-20AT (column, Hypersil BDS C18, 5.0 μm, 4.6 mm×150 mm (Elite); detector, SPD-20A UV/vis detector, UV detection at 254 nm; elution, MeOH in water (60 %, v/v); T = 25 °C; flow rate = 1.0 mL/min).

3-(Hydroxymethyl)-4H-chromen-4-one (**3**). A suspension of formylchromone (5.6 mmol, 974 mg) and basic Al_2O_3 (20 g) in 2-propanol (200 mL) was kept with stirring at 75 ^{o}C for 4 h. The mixture was filtered by celite and the solvent evaporated. The crude material was purified by silica gel column chromatography (petroleum/ethyl acetate, 1:1) to afford **3** (808 mg) as a colorless solid. Yield: 82%; ^{1}H NMR (400 MHz, $CDCl_3$) δ 8.23 (dd, J = 8.0, 1.3 Hz, 1H), 7.96 (s, 1H), 7.72 – 7.67 (m, 1H), 7.47 (d, J = 8.5 Hz, 1H), 7.42 (t, J = 7.6 Hz, 1H), 4.59 (d, J = 5.8 Hz, 2H). The obtained spectra match those reported.[35]

3-(Bromomethyl)-4H-chromen-4-one (**4**). A solution of triphenylphosphine (469

mg, 1.7 mmol) in dry CH_2Cl_2 (2 mL) was added dropwise to a stirred solution of carbon tetrabromide (592 mg, 1.7 mmol) and 3-(hydroxymethyl)-4*H*-chromen-4-one (246 mg, 1.4 mmol) in dry CH_2Cl_2 (11 mL) at room temperature under argon atmosphere. The reaction was stirred for 4 h at room temperature and was concentrated in vacuo to give the crude product. This was purified by silica gel column chromatography (petroleum/ethyl acetate, 2:1) to afford **4** (294 mg) as a colorless solid.[43] Yield: 88 %; ^{1}H NMR (400 MHz, $CDCl_3$) δ 8.26 (dd, J = 8.0, 1.7 Hz, 1H), 8.13 (s, 1H), 7.69 (ddd, J = 8.6, 7.2, 1.7 Hz, 1H), 7.48 – 7.42 (m, 2H), 4.41 (s, 2H).

3-(((5-Methyl-1H-benzo[d]imidazol-2-yl)thio)methyl)-4H-chromen-4-one (**1a**). To 5-methyl-1,3-dihydro-2*H*-benzo[*d*]imidazole-2-thione (656 mg, 4.0 mmol) in dimethylformamide (10 mL), triethylamine (836 µL, 6.0 mmol) and **4** (1434 mg, 6.0 mmol) were added. After stirring at 80 °C overnight, water was added to the mixture followed by extraction with ethyl acetate. After the ethyl acetate phase was dried with anhydrous sodium sulfate, it was concentrated and the residue was purified by silica gel column chromatography (petroleum/ethyl acetate, 1:1) to obtain **1a** (978 mg) as a colorless solid. Yield: 76 %; purity: 99.9 %; ^{1}H NMR (400 MHz, DMSO - d_6) δ 12.41 (d, J = 6.2 Hz, 1H), 8.54 (d, J = 2.0 Hz, 1H), 8.10 (dd, J = 8.0, 1.5 Hz, 1H), 7.81 (ddd, J = 8.6, 7.2, 1.6 Hz, 1H), 7.62 (d, J = 8.5 Hz, 1H), 7.54 – 7.48 (m, 1H), 7.46 – 7.36 (m, 1H), 7.24 – 7.13 (m, 1H), 6.95 (d, J = 8.2 Hz, 1H), 4.29 (s, 2H), 2.38 (d, J = 2.0 Hz, 3H) ; ^{13}C NMR (101 MHz, DMSO - d_6) δ 176.1, 156.3, 155.5, 149.6, 134.7, 133.0, 132.1, 131.1, 126.0, 125.4, 123.6, 123.2, 120.8, 118.9, 110.1, 109.6, 27.0, 21.7; HRMS (ESI-TOF) m/z calcd for $C_{18}H_{14}N_2O_2S$ $[M+H]^+$ 323.0849, found 323.0843.

3-(((5-Methyl-1H-benzo[d]imidazol-2-yl)thio)methyl)-4H-chromen-4-one (**1b**). In a round-bottomed flask (50 mL) equipped with a magnetic stirrer, a solution of **1a** (322 mg, 1.0 mmol) in ethyl acetate (5 mL) was prepared. Oxone was added and the mixture was stirred at room temperature for 24 h. When the starting sulfane had completely disappeared, the mixture was quenched by adding H_2O (10 mL). The product was extracted with ethyl acetate and the combined extracts were dried with anhydrous sodium sulfate. It was concentrated and the residue was purified by silica gel column chromatography (petroleum/ethyl acetate, 1:1) to obtain **1b** (196 mg) as a

colorless solid. Yield: 58 %; purity: 99.4 %; ^{1}H NMR (400 MHz, DMSO - d_6) δ 13.38 (s, 1H), 8.29 (d, J = 11.9 Hz, 1H), 8.01 (d, J = 7.9 Hz, 1H), 7.88 – 7.83 (m, 1H), 7.69 (d, J = 8.4 Hz, 1H), 7.60 – 7.49 (m, 2H), 7.42 – 7.31 (m, 1H), 7.13 (dd, J = 18.5, 8.2 Hz, 1H), 4.48 (d, J = 12.7 Hz, 1H), 4.29 (d, J = 12.8 Hz, 1H), 2.44 (s, 3H); ^{13}C NMR (101 MHz, DMSO - d_6) δ 175.8, 157.5, 156.4, 135.1, 135.0, 126.4, 126.4, 126.2, 125.5, 125.5, 125.4, 123.3, 119.0, 119.0, 113.9, 113.8, 51.1, 21.8; HRMS (ESI-TOF) m/z calcd for $C_{18}H_{14}N_2O_3S$ $[M+H]^+$ 339.0798, found 339.0784.

General Procedures for Synthesis of Compounds 6a-6b. A mixture of 4-oxo-benzopyran-3-carboxaldehyde **2** or **5** (1.0 mmol), meldrum's acid (1.0 mmol) and triethylamine formic acid (1:1) 5 mL was refluxed at 100 ^{o}C for 2 h, until the disappearance of starting material. It was cooled to room temperature and poured into ice water. The mixture was acidified to pH = 2 with 6 N HCl. The pale yellow solid was filtered washed with water and purified by column chromatography. The obtained spectra match those reported. [39]

3-(4-Oxo-4H-chromen-3-yl)propanoic acid (**6a**). Colorless solid. Yield: 93%; ^{1}H NMR (500 MHz, $CDCl_3$) δ 8.23 (dd, J = 8.0, 1.2 Hz, 1H), 7.91 (s, 1H), 7.69 – 7.64 (m, 1H), 7.46 – 7.39 (m, 2H), 2.80 – 2.74 (m, 4H).

3-(6-Chloro-4-oxo-4H-chromen-3-yl)propanoic acid (**6b**). Colorless solid. Yield: 90%; ^{1}H NMR (400 MHz, MeOD) δ 8.14 (s, 1H), 8.06 (d, J = 2.5 Hz, 1H), 7.72 (dd, J = 9.0, 2.6 Hz, 1H), 7.56 (d, J = 9.0 Hz, 1H), 2.74 (t, J = 7.2 Hz, 2H), 2.62 (t, J = 7.2 Hz,2H).

General Procedures for Synthesis of Compounds 7d-7f. A solution of 2-nitroaniline (30.0 mmol) and $SnCl_2{\cdot}2H_2O$ (26.4 g, 109.1 mmol) was heated in ethyl acetate at reflux for 2h, the mixture was then cautiously quenched with saturated sodium bicarbonate aqueous solution. The product was extracted with ethyl acetate and the combined extracts were dried with anhydrous sodium sulfate. It was concentrated and the residue was purified by silica gel column chromatography to give the product.[37]

N^1-benzyl-4-methylbenzene-1,2-diamine (**7d**). Colorless solid. Yield: 45%; ^{1}H NMR (400 MHz, $CDCl_3$) δ 7.44 (dd, J = 13.7, 6.8 Hz, 1H), 7.39 (d, J = 7.2 Hz, 2H), 7.34 (t, J = 7.4 Hz, 2H), 7.29 (dd, J = 9.2, 4.6 Hz, 1H), 6.57 (d, J = 7.0 Hz, 2H), 4.28

(s, 2H), 3.38 (s, 2H), 2.25 – 2.17 (m, 3H).

N^1-(4-fluorobenzyl)-4-methylbenzene-1,2-diamine (**7e**). Colorless solid. Yield: 59%; ^{1}H NMR (500 MHz, $CDCl_3$) δ 7.33 (dd, J = 7.8, 5.6 Hz, 2H), 7.01 (t, J = 8.5 Hz, 2H), 6.63 – 6.49 (m, 3H), 4.24 (d, J = 8.6 Hz, 2H), 3.37 (s, 2H), 2.22 (d, J = 9.3 Hz, 3H).

N^1-(3-fluorobenzyl)-4-methylbenzene-1,2-diamine (**7f**). Colorless solid. Yield: 42%; ^{1}H NMR (400 MHz, $CDCl_3$) δ 7.33 (dd, J = 13.9, 7.8 Hz, 1H), 7.19 (d, J = 7.6 Hz, 1H), 7.14 (d, J = 9.7 Hz, 1H), 6.99 (td, J = 8.4, 2.2 Hz, 1H), 6.62 (d, J = 5.8 Hz, 2H), 6.55 (d, J = 8.4 Hz, 1H), 4.33 (s, 2H), 3.45 (s, 2H), 2.25 (s, 3H).

General Procedures for Synthesis of Compounds 7g-7h. To a mixture of **9d** or **9e** (1.0 mmol) in EtOH (10 mL) was added palladium hydroxide (238 mg, 1.0 mmol) and stirred at room temperature for 6 h under hydrogen atmosphere. The mixture was then filtered through a pad of celite. The filtrate was concentrated in vacuo to give a yellow solid, which was purified by silica gel chromatography (petroleum/ethyl acetate, 10:1) to give **7g-7h** as colorless solid.

3-Amino-5-methyl-2-(pyridin-4-ylamino)benzene-1-ylium (**7g**). Colorless solid.Yield: 89%; ^{1}H NMR (400 MHz, $CDCl_3$) δ 8.24 (dd, J = 4.8, 1.5 Hz, 2H), 7.01 (d, J = 7.9 Hz, 1H), 6.67 (d, J = 1.1 Hz, 1H), 6.62 (dd, J = 7.9, 1.3 Hz, 1H), 6.53 (dd, J = 4.8, 1.5 Hz, 2H), 5.59 (s, 1H), 2.38 – 2.27 (m, 3H).

5-Methyl-N^2-(pyridin-4-yl)pyridine-2,3-diamine (**7h**). Colorless solid. Yield: 81%; ^{1}H NMR (400 MHz, $CDCl_3$) δ 8.30 (d, J = 5.3 Hz, 2H), 7.71 (s, 1H), 7.02 (d, J = 5.3 Hz, 2H), 6.91 (s, 1H), 6.63 (s, 1H), 2.25 (s, 3H).

4-Chloro-N^1-phenylbenzene-1,2-diamine (**7i**). A solution of **13** (30.0 mmol) and $SnCl_2 \cdot 2H_2O$ (26.4 g, 109.1 mmol) was heated in ethyl acetate at reflux for 2 h, the mixture was then cautiously quenched with saturated aqueous $NaHCO_3$. The product was extracted with ethyl acetate and the combined extracts were dried with anhydrous sodium sulfate. It was concentrated and the residue was purified by silica gel column chromatography to give the product (1.9 g). Yield: 30%; ^{1}H NMR (500 MHz, $CDCl_3$) δ 7.21 (t, J = 7.8 Hz, 2H), 7.02 (d, J = 8.3 Hz, 1H), 6.83 (dd, J = 15.6, 8.3 Hz, 1H), 6.78 (d, J = 2.2 Hz, 1H), 6.72 – 6.69 (m, 3H).

General Procedures for Synthesis of Compounds 10a-10e. To a mixture of nitrobenzene (1.0 mmol) in toluene (10 mL) were added aniline (3.0 mmol), tris(dibenzylideneacetone)dipalladium ($Pd_2(dba)_3$, 92 mg, 0.1 mmol), BINAP (23 mg, 0.15 mmol) and cesium carbonate (650 mg, 2.0 mmol). The mixture was then stirred at 110 ^{o}C for 24 h under argon atmosphere. After cooling to room temperature, the mixture was filtered through a pad of celite and the filtrate was then concentrated in vacuo to afford a residue, which was purified by silica gel chromatography (petroleum/ethyl acetate, 50 : 1) to give **10a-10e** as red oil. The obtained spectra match those reported.[38]

N-benzyl-4-methyl-2-nitroaniline (**10a**). Orange oil. Yield: 75%; ^{1}H NMR (400 MHz, $CDCl_3$) δ 8.35 (s, 1H), 8.03 (s, 1H), 7.43 – 7.30 (m, 5H), 7.23 (dd, J = 8.7, 1.8 Hz, 1H), 6.76 (d, J = 8.7 Hz, 1H), 4.56 (d, J = 5.7 Hz, 2H), 2.28 (s, 3H).

N-(4-fluorobenzyl)-4-methyl-2-nitroaniline (**10b**). Orange oil. Yield: 68%; ^{1}H NMR (400 MHz, $CDCl_3$) δ 8.28 (s, 1H), 8.00 (s, 1H), 7.31 (dd, J = 8.4, 5.4 Hz, 2H), 7.22 (dd, J = 8.7, 1.8 Hz, 1H), 7.04 (t, J = 8.6 Hz, 2H), 6.69 (d, J = 8.7 Hz, 1H), 4.50 (d, J = 5.7 Hz, 2H), 2.26 (s, 3H).

N-(3-fluorobenzyl)-4-methyl-2-nitroaniline (**10c**). Orange oil. Yield: 82%; ^{1}H NMR (400 MHz, $CDCl_3$) δ 8.33 (s, 1H), 7.99 (s, 1H), 7.31 (dd, J = 13.9, 7.8 Hz, 1H), 7.20 (d, J = 8.7 Hz, 1H), 7.12 (d, J = 7.6 Hz, 1H), 7.03 (d, J = 9.6 Hz, 1H), 6.97 (t, J = 8.4 Hz, 1H), 6.66 (d, J = 8.7 Hz, 1H), 4.53 (d, J = 5.8 Hz, 2H), 2.25 (s, 3H).

5-Methyl-3-nitro-N-(pyridin-4-yl)pyridin-2-amine (**10d**). Red oil. Yield: 53%; ^{1}H NMR (400 MHz, $CDCl_3$) δ 10.13 (s, 1H), 8.51 (s, 2H), 8.43 (d, J = 9.0 Hz, 1H), 8.38 (d, J = 8.2 Hz, 1H), 7.69 (s, 2H), 2.38 (d, J = 9.1 Hz, 3H).

N-(4-methyl-2-nitrophenyl)pyridin-4-amine (**10e**). Orange oil. Yield: 55%; ^{1}H NMR (400 MHz, $CDCl_3$) δ 9.09 (s, 1H), 8.49 (d, J = 5.8 Hz, 2H), 8.03 (d, J = 1.1 Hz, 1H), 7.53 (d, J = 8.6 Hz, 1H), 7.38 (dd, J = 8.6, 2.0 Hz, 1H), 7.09 (dd, J = 4.8, 1.4 Hz, 2H), 2.45 – 2.35 (m, 3H).

4-Chloro-2-nitro-N-phenylaniline (**13**). Aniline (930 mg, 10.0 mmol), and potassium carbonate (2.7 g, 20.0 mmol) were added to a solution of 1,4-dichloro-2-nitrobenzene (1.9 g, 10.0 mmol) and DMSO. The resulting mixture was stirred at about

120 °C for about 16 h, and then the solvent was removed by evaporation in vacuo. Following standard extractive workup with dichloromethane (2×100 mL), the crude residue was purified by silica gel column chromatography (dichloromethane/methanol, 20:1) to give the title product as a yellow solid (868 mg). Yield: 35%; ^{1}H NMR (400 MHz, $CDCl_3$) δ 9.45 (s, 1H), 8.23 – 8.19 (m, 1H), 7.48 – 7.40 (m, 3H), 7.33 – 7.28 (m, 2H), 7.25 (s, 1H), 7.18 – 7.14 (m, 1H).

General Procedures for Synthesis of Compounds 1c-1k. To a mixture of appropriate amine (1.0 mmol) in CH_2Cl_2 (15 mL) were added HATU (570 mg, 1.5 mmol), *N*, *N*-diisopropylethylamine (516 mg, 4.0 mmol) and **6a or 6b** (1.2 mmol), and stirred at room temperature for 12 h. The mixture was diluted with saturated sodium bicarbonate aqueous solution (100 mL) and extracted with dichloromethane (300 mL). The organic layer was washed with brine, dried over anhydrous sodium sulfate, filtered and concentrated in vacuo. To the residue was added acetic acid (20 mL), and stirred at 90 °C for 12 h. Then the reaction mixture was concentrated in vacuo. The residue was diluted with saturated sodium bicarbonate aqueous solution and extracted with dichloromethane. The organic layer was washed with brine, dried over anhydrous sodium sulfate, filtered and concentrated in vacuo. The residue was purified by silica gel column chromatography (petroeum/ethyl acetate, 10:1) to give compound **1c-1k** as a colorless solid.[40]

6-Chloro-3-(2-(5-methyl-1H-benzo[d]imidazol-2-yl)ethyl)-4H-chromen-4-one (**1c**). Colorless solid. Yield: 45%; purity: 99.7%; ^{1}H NMR (500 MHz, $CDCl_3$) δ 8.10 (s, 1H), 7.93 (s, 1H), 7.59 – 7.55 (m, 1H), 7.43 (d, J = 8.2 Hz, 1H), 7.36 (d, J = 8.9 Hz, 1H), 7.32 (s, 1H), 7.04 (d, J = 8.2 Hz, 1H), 3.29 (t, J = 7.1 Hz, 2H), 3.03 (t, J = 7.0 Hz, 2H), 2.45 (s, 3H); ^{13}C NMR (126 MHz, $CDCl_3$) δ 177.3, 154.8, 154.1, 153.5, 134.0×2, 132.3, 131.1, 124.9, 124.5, 123.9, 123.0, 120.0×2, 114.5, 114.1, 28.0, 24.6, 21.6; HRMS (ESI-TOF) m/z calcd for $C_{19}H_{15}N_2O_2Cl$ $[M+H]^+$ 339.0895, found 339.0895.

3-(2-(5-Methoxy-1H-benzo[d]imidazol-2-yl)ethyl)-4H-chromen-4-one (**1d**). Colorless solid. Yield: 53%; purity: 99.9%; ^{1}H NMR (500 MHz, $CDCl_3$) δ 8.15 (d, J = 8.0 Hz, 1H), 7.89 (s, 1H), 7.62 (t, J = 7.7 Hz, 1H), 7.40 (dd, J = 13.9, 8.5 Hz, 2H), 7.34 (t, J = 7.5 Hz, 1H), 7.01 (s, 1H), 6.83 (d, J = 8.7 Hz, 1H), 3.81 (s, 3H), 3.24 (t, J = 7.2

Hz, 2H), 3.02 (t, J = 7.2 Hz, 2H); ^{13}C NMR (101 MHz, $CDCl_3$) δ 178.4, 156.5, 156.0, 154.0, 153.7×2, 133.7×2, 125.4×2, 125.1×2, 123.6, 122.9, 118.2, 111.3, 55.8, 28.3, 24.9; HRMS (ESI-TOF) m/z calcd for $C_{19}H_{16}N_2O_3$ $[M+H]^+$ 321.1234, found 321.1212.

3-(2-(5-(Trifluoromethyl)-1H-benzo[d]imidazol-2-yl)ethyl)-4H-chromen-4-one (**1e**). Colorless solid. Yield: 44%; purity: 99.9%; ^{1}H NMR (400 MHz, Acetone - *d6*) δ 8.14 (d, J = 10.7 Hz, 2H), 7.90 (s, 1H), 7.76 (t, J = 7.8 Hz, 2H), 7.61 (d, J = 7.5 Hz, 1H), 7.50 (d, J = 8.5 Hz, 1H), 7.49 – 7.44 (m, 2H), 3.28 (t, J = 7.3 Hz, 2H), 3.04 (t, J = 7.3 Hz, 2H); ^{13}C NMR (101 MHz, DMSO - d_6) δ 177.0, 157.6, 156.4, 154.3, 134.4, 127.0, 125.7, 125.5, 124.3, 123.6, 122.9, 122.8, 122.6, 122.3, 121.9, 118.8, 118.5, 27.8, 24.3; HRMS (ESI-TOF) m/z calcd for C_{19} H_{13} N_2 O_2 F_3 $[M+H]^+$ 359.1002, found 359.1000.

3-(2-(1-Benzyl-5-methyl-1H-benzo[d]imidazol-2-yl)ethyl)-4H-chromen-4-one (**1f**). Colorless solid. Yield: 64%; purity: 98.9%; ^{1}H NMR (500 MHz, $CDCl_3$) δ 8.17 (d, J = 7.8 Hz, 1H), 7.88 (s, 1H), 7.63 (t, J = 7.7 Hz, 1H), 7.55 (s, 1H), 7.37 (t, J = 8.1 Hz, 2H), 7.14 (dd, J = 15.7, 8.4 Hz, 3H), 7.09 (d, J = 8.3 Hz, 1H), 7.00 (dd, J = 13.2, 7.8 Hz, 3H), 5.36 (s, 2H), 3.18 (t, J = 7.3 Hz, 2H), 3.03 (t, J = 7.3 Hz, 2H), 2.47 (s, 3H); ^{13}C NMR (101 MHz, $CDCl_3$) δ 177.9, 156.5, 154.4, 153.4, 143.0, 136.2, 133.5, 133.5, 131.7, 128.8×2, 127.6, 126.2×2, 125.7, 124.9, 123.9, 123.8, 122.8, 119.1, 118.1, 109.3, 46.9, 26.3, 24.8, 21.6; HRMS (ESI-TOF) m/z calcd for $C_{26}H_{22}N_2O_2$ $[M+H]^+$ 395.1754, found 395.1726.

3-(2-(1-(4-Fluorobenzyl)-5-methyl-1H-benzo[d]imidazol-2-yl)ethyl)-4H-chromen-4-one (**1g**). Colorless solid. Yield: 48%; purity: 99.7%; ^{1}H NMR (500 MHz, $CDCl_3$) δ 8.15 (d, J = 8.0 Hz, 1H), 7.88 (s, 1H), 7.63 (t, J = 7.8 Hz, 1H), 7.55 (s, 1H), 7.38 (d, J = 7.9 Hz, 2H), 7.04 (dd, J = 22.5, 8.0 Hz, 2H), 6.97 (d, J = 14.7 Hz, 2H), 6.80 (t, J = 7.9 Hz, 2H), 5.33 (s, 2H), 3.18 (t, J = 7.2 Hz, 2H), 3.02 (t, J = 7.1 Hz, 2H), 2.45 (d, J = 20.6 Hz, 3H); ^{13}C NMR (101 MHz, $CDCl_3$) δ 177.9, 156.4, 154.3, 153.4, 143.0, 133.5×2, 133.3, 132.0, 131.8, 127.9, 127.9, 125.6×2, 125.0, 123.9, 122.7, 119.2, 118.1, 115.8, 115.6, 109.2, 46.2, 26.2, 25.0, 21.6; HRMS (ESI-TOF) m/z calcd for $C_{26}H_{21}N_2O_2F$ $[M+H]^+$ 413.1660, found 413.1660.

3-(2-(1-(3-Fluorobenzyl)-5-methyl-1H-benzo[d]imidazol-2-yl)ethyl)-4H-

chromen-4-one (**1h**). Colorless solid. Yield: 50%; purity: 98.4%; ^{1}H NMR (400 MHz, $CDCl_3$) δ 8.17 (d, J = 7.9 Hz, 1H), 7.89 (s, 1H), 7.64 (t, J = 7.8 Hz, 1H), 7.56 (s, 1H), 7.38 (t, J = 8.1 Hz, 2H), 7.14 – 7.02 (m, 3H), 6.79 (dd, J = 16.6, 8.0 Hz, 2H), 6.69 (d, J = 9.4 Hz, 1H), 5.37 (s, 2H), 3.18 (t, J = 7.3 Hz, 2H), 3.02 (t, J = 7.2 Hz, 2H), 2.48 (s, 3H); ^{13}C NMR (101 MHz, $CDCl_3$) δ 177.9, 156.5, 154.3, 153.3, 143.1, 133.5, 133.3, 131.9, 130.5, 130.4, 125.7, 125.0, 123.9, 122.7, 121.8, 119.3, 118.2, 114.7, 114.5, 113.4, 113.2, 109.1, 46.4, 26.2, 25.0, 21.6; HRMS (ESI-TOF) m/z calcd for $C_{26}H_{21}N_2O_2F$ $[M+H]^+$ 413.1660, found 413.1652.

3-(2-(5-Methyl-1-phenyl-1H-benzo[d]imidazol-2-yl)ethyl)-4H-chromen-4-one (**1i**). Colorless solid. Yield: 42%; purity: 99.8%; ^{1}H NMR (500 MHz, $CDCl_3$) δ 8.12 (dd, J = 8.0, 1.5 Hz, 1H), 7.82 (s, 1H), 7.64 – 7.60 (m, 1H), 7.58 (s, 1H), 7.44 – 7.33 (m, 5H), 7.24 – 7.19 (m, 2H), 7.01 (t, J = 9.2 Hz, 1H), 6.97 (d, J = 8.2 Hz, 1H), 3.14 (t, J = 7.1 Hz, 2H), 3.02 (t, J = 6.9 Hz, 2H), 2.49 (s, 3H). ^{13}C NMR (126 MHz, $CDCl_3$) δ 177.5, 156.4, 154.2, 153.1, 142.8, 135.7, 134.5, 133.4, 132.1, 129.8×2, 128.7, 127.1×2, 125.8, 124.9, 124.1, 123.9, 122.9, 118.9, 118.1, 109.6, 26.4, 24.6, 21.6; HRMS (ESI-TOF) m/z calcd for $C_{25}H_{20}N_2O_2$ $[M+H]^+$ 381.1598, found 381.1598 .

3-(2-(5-Methyl-1-(pyridin-4-yl)-1H-benzo[d]imidazol-2-yl)ethyl)-4H-chromen-4-one (**1j**). Colorless solid. Yield: 55%; purity: 97.7%;^{1}H NMR (400 MHz, $CDCl_3$) δ 8.72 (d, J = 5.0 Hz, 2H), 8.13 (d, J = 7.8 Hz, 1H), 7.86 (s, 1H), 7.64 (t, J = 7.5 Hz, 1H), 7.59 (s, 1H), 7.38 (t, J = 7.6 Hz, 2H), 7.26 (s, 2H), 7.07 (s, 2H), 3.21 (t, J = 7.1 Hz, 2H), 3.05 (t, J = 7.1 Hz, 2H), 2.50 (s, 3H). ^{13}C NMR (101 MHz, $CDCl_3$) δ 177.6, 156.4, 153.4, 153.2, 151.7×2, 143.5, 143.1, 133.6, 133.2, 133.0, 125.8, 125.1, 124.7, 123.8, 122.6, 121.2×2, 119.4, 118.1, 109.4, 26.5, 24.8, 21.5; HRMS (ESI-TOF) m/z calcd for $C_{24}H_{19}N_3O_2$ $[M+H]^+$ 382.1550, found 382.1540 .

3-(2-(5-Chloro-1-phenyl-1H-benzo[d]imidazol-2-yl)ethyl)-4H-chromen-4-one (**1k**). Colorless solid. Yield: 44%; purity: 96.9%; ^{1}H NMR (400 MHz, $CDCl_3$) δ 8.14 (dd, J = 8.0, 1.3 Hz, 1H), 7.86 (s, 1H), 7.78 (d, J = 1.7 Hz, 1H), 7.67 – 7.63 (m, 1H), 7.49 – 7.45 (m, 3H), 7.43 – 7.37 (m, 2H), 7.24 (dd, J = 6.5, 2.9 Hz, 2H), 7.17 (dd, J = 8.6, 1.8 Hz, 1H), 7.01 (d, J = 8.6 Hz, 1H), 3.15 (t, J = 7.0 Hz, 2H), 3.04 (t, J = 7.1 Hz, 2H); ^{13}C NMR (126 MHz, $CDCl_3$) δ 177.5, 156.4, 155.6, 153.2, 143.4, 135.1, 135.0,

133.5, 130.0×2, 129.1, 128.0, 127.1×2, 125.7, 124.9, 123.9, 123.1, 122.7, 118.9, 118.1, 110.9, 26.4, 24.4; HRMS (ESI-TOF) m/z calcd for $C_{24}H_{17}N_2O_2Cl$ $[M+H]^+$ 401.1051, found 401.1017 .

General Procedures for Synthesis of Compounds 15a-15e. 15a-15e was synthesized by the general procedure for synthesis of **6a-6b**.

3-(6-Fluoro-4-oxo-4H-chromen-3-yl)propanoic acid (**15a**). Colorless solid. Yield: 88%; ^{1}H NMR (400 MHz, MeOD) δ 8.16 (d, J = 0.7 Hz, 1H), 7.79 – 7.73 (m, 1H), 7.62 (ddd, J = 9.2, 4.2, 1.5 Hz, 1H), 7.55 (tdd, J = 9.2, 3.1, 1.4 Hz, 1H), 2.75 (t, J = 7.2 Hz, 2H), 2.65 – 2.58 (m, 2H).

3-(6-Chloro-4-oxo-4H-chromen-3-yl)propanoic acid (**15b**). Colorless solid. Yield: 85%; ^{1}H NMR (400 MHz, MeOD) δ 8.14 (s, 1H), 8.06 (d, J = 2.5 Hz, 1H), 7.72 (dd, J = 9.0, 2.6 Hz, 1H), 7.56 (d, J = 9.0 Hz, 1H), 2.74 (t, J = 7.2 Hz, 2H), 2.62 (t, J = 7.2 Hz, 2H).

3-(6-Bromo-4-oxo-4H-chromen-3-yl)propanoic acid (**15c**). Colorless solid. Yield: 92%; ^{1}H NMR (400 MHz, $CDCl_3$) δ 8.34 (d, J = 2.2 Hz, 1H), 7.90 (s, 1H), 7.77 – 7.70 (m, 1H), 7.34 (dd, J = 8.9, 2.1 Hz, 1H), 2.85 – 2.68 (m, 4H).

3-(6-Iodo-4-oxo-4H-chromen-3-yl)propanoic acid (**15d**). Colorless solid. Yield: 85%; ^{1}H NMR (400 MHz, $CDCl_3$) δ 8.55 (d, J = 2.2 Hz, 1H), 7.92 (dd, J = 8.6, 2.3 Hz, 2H), 7.22 (d, J = 8.8 Hz, 1H), 2.80 – 2.72 (m, 4H).

3-(6-Methoxy-4-oxo-4H-chromen-3-yl)propanoic acid (**15e**). Colorless solid. Yield: 80%; ^{1}H NMR (500 MHz, $CDCl_3$) δ 7.90 (s, 1H), 7.57 (d, J = 3.1 Hz, 1H), 7.39 – 7.36 (m, 1H), 7.25 (dd, J = 9.2, 3.1 Hz, 1H), 3.89 (d, J = 4.5 Hz, 3H), 2.80 – 2.77 (m, 2H), 2.74 (dd, J = 7.9, 4.2 Hz, 2H).

General Procedures for Synthesis of Compounds 2a-2e. 2a-2e was synthesized by the general procedure for synthesis of **1c-1k**.

6-Fluoro-3-(2-(5-methyl-1-phenyl-1H-benzo[d]imidazol-2-yl)ethyl)-4H-chromen-4-one (**2a**). Colorless solid. Yield: 60%; purity: 99.7%; ^{1}H NMR (500 MHz, $CDCl_3$) δ 7.84 (s, 1H), 7.74 (dd, J = 8.3, 2.6 Hz, 1H), 7.57 (s, 1H), 7.44 (d, J = 6.8 Hz, 3H), 7.41 – 7.33 (m, 2H), 7.22 (d, J = 7.4 Hz, 2H), 7.02 (d, J = 8.2 Hz, 1H), 6.97 (d, J = 8.2 Hz, 1H), 3.13 (t, J = 7.0 Hz, 2H), 3.01 (t, J = 7.0 Hz, 2H), 2.49 (s, 3H); ^{13}C NMR

(101 MHz, $CDCl_3$) δ 176.9, 154.0, 153.4, 142.8, 135.7, 134.5, 132.2, 129.9×2, 128.7, 127.1×2, 124.1, 122.3, 121.8, 121.6, 120.2, 120.1, 118.9, 110.6, 110.4, 109.7, 26.3, 24.40, 21.6; HRMS (ESI-TOF) m/z calcd for $C_{25}H_{19}N_2O_2F$ $[M+H]^+$ 399.1503, found 399.1482 .

6-Chloro-3-(2-(5-methyl-1-phenyl-1H-benzo[d]imidazol-2-yl)ethyl)-4H-chromen-4-one (**2b**). Colorless solid. Yield: 45%; purity: 99.9%; ^{1}H NMR (500 MHz, $CDCl_3$) δ 8.06 (d, J = 2.1 Hz, 1H), 7.83 (s, 1H), 7.58 – 7.53 (m, 2H), 7.43 (d, J = 6.9 Hz, 3H), 7.33 (d, J = 8.9 Hz, 1H), 7.22 (d, J = 6.5 Hz, 2H), 7.01 (d, J = 8.2 Hz, 1H), 6.97 (d, J = 8.2 Hz, 1H), 3.12 (t, J = 7.0 Hz, 2H), 3.01 (t, J = 7.0 Hz, 2H), 2.48 (s, 3H); ^{13}C NMR (101 MHz, $CDCl_3$) δ 176.4, 154.7, 154.0, 153.3, 142.8, 135.7, 134.48, 133.60, 132.12, 130.78, 129.85×2, 128.72, 127.07×2, 125.14, 124.74, 124.10, 123.0, 119.8, 119.0, 109.7, 26.2, 24.4, 21.6; HRMS (ESI-TOF) m/z calcd for $C_{25}H_{19}N_2O_2Cl$ $[M+H]^+$ 415.1208, found 415.1210 .

6-Bromo-3-(2-(5-methyl-1-phenyl-1H-benzo[d]imidazol-2-yl)ethyl)-4H-chromen-4-one (**2c**). Colorless solid. Yield: 59%; purity: 99.5%; ^{1}H NMR (500 MHz, $CDCl_3$) δ 8.22 (d, J = 2.3 Hz, 1H), 7.83 (s, 1H), 7.70 – 7.67 (m, 1H), 7.57 (s, 1H), 7.47 – 7.41 (m, 3H), 7.29 – 7.26 (m, 1H), 7.22 (dd, J = 7.5, 1.6 Hz, 2H), 6.99 (dd, J = 22.8, 8.2 Hz, 2H), 3.12 (t, J = 7.1 Hz, 2H), 3.00 (t, J = 7.0 Hz, 2H), 2.48 (s, 3H); ^{13}C NMR (126 MHz, $CDCl_3$) δ 176.2, 155.1, 153.9, 153.3, 142.7, 136.3, 135.7, 134.5, 132.2, 129.9×2, 128.7, 128.4, 127.1×2, 125.1, 124.1, 123.1, 120.1, 118.9, 118.2, 109.7, 26.2, 24.4, 21.6; HRMS (ESI-TOF) m/z calcd for $C_{25}H_{19}N_2O_2Br$ $[M+H]^+$ 459.0703, found 459.0690 .

6-Iodo-3-(2-(5-methyl-1-phenyl-1H-benzo[d]imidazol-2-yl)ethyl)-4H-chromen-4-one (**2d**). Colorless solid. Yield: 46%; purity: 97.9%; ^{1}H NMR (500 MHz, $CDCl_3$) δ 8.46 – 8.39 (m, 1H), 7.90 – 7.79 (m, 2H), 7.55 (d, J = 17.1 Hz, 1H), 7.43 (s, 3H), 7.29 – 7.24 (m, 1H), 7.21 (d, J = 3.1 Hz, 2H), 7.17 – 7.10 (m, 1H), 7.04 – 6.95 (m, 2H), 3.13 (d, J = 3.6 Hz, 2H), 3.00 (d, J = 3.5 Hz, 2H), 2.48 (d, J = 3.5 Hz, 3H); ^{13}C NMR (126 MHz, $CDCl_3$) δ 176.0, 155.8, 153.9, 153.3, 142.5, 141.9, 135.6, 134.7, 134.4, 132.3, 129.9×2, 128.8, 127.1×2, 125.5, 124.2, 123.2, 120.2, 118.8, 109.7, 88.6, 26.2, 24.5, 21.6; HRMS (ESI-TOF) m/z calcd for $C_{25}H_{19}N_2O_2I$ $[M+H]^+$ 507.0564, found 507.0542

.

6-Methoxy-3-(2-(5-methyl-1-phenyl-1H-benzo[d]imidazol-2-yl)ethyl)-4H-chromen-4-one (**2e**). Colorless solid. Yield: 50%; purity: 99.9%; ^{1}H NMR (500 MHz, $CDCl_3$) δ 7.81 (s, 1H), 7.58 (s, 1H), 7.48 – 7.39 (m, 4H), 7.31 (d, J = 9.1 Hz, 1H), 7.22 (t, J = 8.0 Hz, 3H), 7.01 (d, J = 8.2 Hz, 1H), 6.97 (d, J = 8.2 Hz, 1H), 3.87 (s, 3H), 3.13 (t, J = 7.1 Hz, 2H), 3.02 (t, J = 7.1 Hz, 2H), 2.49 (s, 3H); ^{13}C NMR (101 MHz, $CDCl_3$) δ 177.3, 156.7, 154.2, 152.9, 151.3, 142.9, 135.8, 134.5, 132.1, 129.8×2, 128.6, 127.1×2, 124.4, 124.0, 123.6, 122.1, 119.5, 119.0, 109.6, 104.7, 55.9, 26.5, 24.6, 21.6; HRMS (ESI-TOF) m/z calcd for $C_{26}H_{22}N_2O_3$ $[M+H]^+$ 411.1703, found 411.1713 .

General Procedures for Synthesis of Compounds 16a-16c. A mixture of 4-oxo-4*H*-chromene-3-carbaldehyde (174 mg, 1.0 mmol) and malonic acid (208 mg, 2.0 mmol) in the presence of pyridine (5 mL) was refluxed for 45 min with vigorous stirring. Upon completion, the mixture was cooled to room temperature, the pH adjusted to 1.0 with concentrated HCl, and the reaction was stirred for additional 30 min. The yellow colored solid was filtered, washed with 1 M HCl (2 × 20 mL), and dried. The compound was obtained and recrystallized from MeOH. The obtained spectra match those reported. [42]

(E)-3-(4-oxo-4H-chromen-3-yl)acrylic acid (**16a**). Colorless solid. Yield: 85%; ^{1}H NMR (400 MHz, DMSO - d_6) δ 8.87 (s, 1H), 8.14 (d, J = 7.9 Hz, 1H), 7.85 (t, J = 7.7 Hz, 1H), 7.71 (d, J = 8.4 Hz, 1H), 7.55 (t, J = 7.5 Hz, 1H), 7.43 (d, J = 15.9 Hz, 1H), 7.12 (d, J = 15.9 Hz, 1H).

(E)-3-(6-fluoro-4-oxo-4H-chromen-3-yl)acrylic acid (**16b**). Colorless solid. Yield: 92%; ^{1}H NMR (500 MHz, DMSO - d_6) δ 12.43 (s, 1H), 8.88 (s, 1H), 7.83 – 7.70 (m, 3H), 7.41 (d, J = 15.9 Hz, 1H), 7.09 (d, J = 15.9 Hz, 1H).

(E)-3-(6-chloro-4-oxo-4H-chromen-3-yl)acrylic acid (**16c**). Colorless solid. Yield: 82%; ^{1}H NMR (400 MHz, DMSO - d_6) δ 8.86 (s, 1H), 8.01 (s, 1H), 7.85 (d, J = 9.0 Hz, 1H), 7.75 (d, J = 8.9 Hz, 1H), 7.39 (d, J = 16.0 Hz, 1H), 7.08 (d, J = 15.9 Hz, 1H).

General Procedures for Synthesis of Compounds 3a-3f. 3a-3f was synthesized by the general procedure for synthesis of **1c-1k**.

(E)-3-(2-(5-methyl-1-phenyl-1H-benzo[d]imidazol-2-yl)vinyl)-4H-chromen-4-

one (**3a**). Colorless solid. Yield: 43%; purity: 98.3%; ^{1}H NMR (500 MHz, $CDCl_3$) δ 8.22 (d, J = 7.9 Hz, 1H), 8.14 (s, 1H), 8.00 (d, J = 15.6 Hz, 1H), 7.69 – 7.60 (m, 5H), 7.55 (t, J = 7.3 Hz, 1H), 7.47 (t, J = 7.3 Hz, 3H), 7.41 (t, J = 7.6 Hz, 1H), 7.11 (d, J = 8.3 Hz, 1H), 7.05 (d, J = 8.2 Hz, 1H), 2.50 (s, 3H); ^{13}C NMR (126 MHz, $CDCl_3$) δ 176.7, 156.8, 155.5, 151.3, 143.3, 135.6, 134.7, 133.7, 132.9, 129.9×2, 128.9, 127.9, 127.3×2, 126.2, 125.5, 124.6, 124.2, 120.4, 119.0, 118.7, 118.1, 109.9, 21.7; HRMS (ESI-TOF) m/z calcd for $C_{25}H_{18}N_2O_2$ $[M+H]^+$ 379.1441, found 379.1423 .

(E)-3-(2-(6-methyl-3-phenyl-3H-imidazo[4,5-b]pyridin-2-yl)vinyl)-4H-chromen-4-one (**3b**). Colorless solid. Yield: 34%; purity: 99.6%; ^{1}H NMR (400 MHz, $CDCl_3$) δ 8.23 (dd, J = 8.0, 1.3 Hz, 1H), 8.18 (s, 1H), 8.14 (s, 1H), 8.05 (d, J = 15.6 Hz, 1H), 7.86 (s, 1H), 7.72 – 7.69 (m, 1H), 7.68 – 7.62 (m, 3H), 7.57 – 7.53 (m, 2H), 7.52 – 7.46 (m, 2H), 7.42 (t, J = 7.5 Hz, 1H), 2.49 (s, 3H); ^{13}C NMR (101 MHz, $CDCl_3$) δ 176.4, 157.0, 155.4, 152.3, 147.4, 145.2, 135.4, 134.2, 133.8, 129.2×2, 129.0, 128.9, 128.8, 127.7×2, 126.6, 126.2, 125.6, 124.2, 120.2, 118.6, 118.1, 18.8; HRMS (ESI-TOF) m/z calcd for $C_{24}H_{17}N_3O_2$ $[M+H]^+$ 380.1394, found 380.1379 .

(E)-3-(2-(5-chloro-1-phenyl-1H-benzo[d]imidazol-2-yl)vinyl)-4H-chromen-4-one (**3c**). Colorless solid. Yield: 38%; purity: 96.9%; ^{1}H NMR (500 MHz, $CDCl_3$) δ 8.22 (d, J = 8.0 Hz, 1H), 8.15 (s, 1H), 8.00 (d, J = 15.6 Hz, 1H), 7.78 (s, 1H), 7.70 – 7.63 (m, 4H), 7.59 (d, J = 7.2 Hz, 1H), 7.46 (dd, J = 13.8, 8.2 Hz, 3H), 7.41 (t, J = 7.6 Hz, 1H), 7.18 (d, J = 8.6 Hz, 1H), 7.12 (d, J = 8.6 Hz, 1H); ^{13}C NMR (126 MHz, $CDCl_3$) δ 176.4, 157.1, 155.5, 152.7, 143.9, 135.2, 135.0, 133.8, 130.1×2, 129.3, 129.0, 128.7, 127.3×2, 126.2, 125.6, 124.2, 123.5, 120.1, 118.9, 118.2, 118.2, 111.1; HRMS (ESI-TOF) m/z calcd for $C_{24}H_{15}N_2O_2Cl$ $[M+H]^+$ 399.0895, found 399.0914 .

(E)-6-chloro-3-(2-(5-methyl-1-phenyl-1H-benzo[d]imidazol-2-yl)vinyl)-4H-chromen-4-one (**3d**). Colorless solid. Yield: 41%; purity: 94.9%; ^{1}H NMR (400 MHz, $CDCl_3$) δ 8.21 (d, J = 2.3 Hz, 1H), 8.14 (s, 1H), 7.99 (d, J = 15.7 Hz, 1H), 7.68 – 7.57 (m, 6H), 7.49 – 7.43 (m, 3H), 7.13 (d, J = 8.2 Hz, 1H), 7.07 (d, J = 8.3 Hz, 1H), 2.52 (s, 3H); ^{13}C NMR (101 MHz, $CDCl_3$) δ 175.5, 156.7, 153.9, 151.1, 143.3, 135.6, 134.7, 133.9, 133.0, 131.6, 130.0×2, 128.9, 127.3×2, 127.2, 125.6, 125.1, 124.8, 120.5, 119.9, 119.2, 119.0, 109.9, 21.7; HRMS (ESI-TOF) m/z calcd for C_{25} H_{17} N_2 O_2 Cl

[M+H]$^+$ 413.1051, found 413.1025.

(E)-3-(2-(5-chloro-1-phenyl-1H-benzo[d]imidazol-2-yl)vinyl)-6-fluoro-4H-chromen-4-one (**3e**). Colorless solid. Yield: 40%; purity: 98.6%; ^{1}H NMR (400 MHz, DMSO - d_6) δ 8.92 (s, 1H), 7.85 (d, J = 15.5 Hz, 2H), 7.78 – 7.68 (m, 7H), 7.58 (d, J = 7.1 Hz, 2H), 7.25 (d, J = 8.4 Hz, 1H), 7.18 (d, J = 8.4 Hz, 1H); ^{13}C NMR (101 MHz, $CDCl_3$) δ 175.6, 157.1, 152.5, 151.7, 143.9, 135.2, 135.0, 130.1×2, 129.3, 128.7, 128.5, 127.3×2, 123.5, 122.2, 122.0, 120.4, 120.3, 119.5, 119.0, 118.6, 111.1, 110.9; HRMS (ESI-TOF) m/z calcd for $C_{24}H_{14}N_2O_2FCl$ [M+H]$^+$ 417.0801, found 417.0781.

(E)-6-chloro-3-(2-(5-chloro-1-phenyl-1H-benzo[d]imidazol-2-yl)vinyl)-4H-chromen-4-one (**3f**). Colorless solid. Yield: 35%; purity: 99.7%; ^{1}H NMR (400 MHz, $CDCl_3$) δ 8.20 (d, J = 2.5 Hz, 1H), 8.15 (s, 1H), 8.03 – 7.97 (m, 1H), 7.79 (d, J = 15 Hz, 1H), 7.70 – 7.60 (m, 5H), 7.46 (dd, J = 8.0, 3.4 Hz, 3H), 7.21 (dd, J = 8.6, 1.7 Hz, 1H), 7.14 (d, J = 8.6 Hz, 1H); ^{13}C NMR (101 MHz, $CDCl_3$) δ 175.2, 157.0, 153.7, 152.4, 143.9, 135.2, 135.0, 134.0, 131.6, 130.1×2, 129.3, 128.7, 128.3, 127.3×2, 125.6, 125.1, 123.5, 120.2, 119.9, 119.0, 118.7, 111.1; HRMS (ESI-TOF) m/z calcd for $C_{24}H_{14}N_2O_2Cl_2$ [M+H]$^+$ 433.0505, found 433.0482.

Protein Expression and Purification

The recombinant PDE10A catalytic domain (residues 449-770) was expressed and purified by using previously reported protocols.[31,44] Briefly, the plasmid (pET15b-PDE10A) was transferred to *E. coli* strain BL21 (Codonplus, Stratagene). Then, the *E. coli* cells carrying the recombinant plasmid were grown in 2XYT medium (containing 100 μg/mL ampicillin and 30 μg/mL chloramphenicol) at 37 °C until an absorption of OD_{600} = 0.6 ~ 0.8. Then, 1 mM isopropyl-β-D-thiogalactopyranoside was added to induce the expression of the PDE10A protein and the culture was incubated at 15 °C for 48 h. The catalytic domain of PDE10A was purified with three chromatographic columns of nickel-nitrilotriacetic acid (Qiagen), Q-Sepharose (Amersham Biosciences), and Sephacryl S300 (GE Healthcare). The nickel-nitrilotriacetic acid affinity column was washed with 15 mM imidazole and eluted with a buffer of 20 mM Tris base, pH = 7.5, 50 mM NaCl, 150 mM imidazole, and 1 mM β-mercaptoethanol. After removal of the His tag by thrombin cleavage, the PDE10A

catalytic domain was loaded into a Q-Sepharose column and eluted with 20 mM Tris base, pH = 7.5, 200 mM NaCl, 1 mM β-ME and 1 mM EDTA. The PDE10A was finally purified by passing through a Sephacryl S300 column in a buffer of 20 mM Tris base, pH = 7.5, 50 mM NaCl, 1 mM β-ME and 1 mM EDTA. A typical batch of purification yielded about 10 mg of PDE10A from 10 liters of cell culture. Purified protein showed a single band in SDS-PAGE and is estimated to have purity over 95%. The catalytic domains of PDE1B (10-487), PDE2A (580-919), PDE3A (679-1087), PDE4D (86-413), PDE7A (130-482), PDE8A (480-820) and PDE9A (181-506), were purified by using similar protocols as previously reported.[31,44]

Enzymatic Assays

The enzymatic activities of the catalytic domain of PDE10A2 were measured with ^{3}H-cAMP (20,000-30,000 cpm, GE Healthcare) as the substrate in a buffer composed of 50 mM Tris, pH = 7.5, 4 mM $MgCl_2$ and 1 mM dithiothreitol. The enzymatic reaction was performed at room temperature for 15 min and then terminated by the addition of 0.2 M $ZnSO_4$. The reaction product was precipitated by the addition of 0.2 N $Ba(OH)_2$ and the unreacted ^{3}H-cAMP remained in the supernatant. The radioactivity in the supernatant was measured in 2.5 mL of Ultima Gold liquid scintillation cocktails (PerkinElmer) with a PerkinElmer 2910 liquid scintillation counter. At least eight concentrations of inhibitors were used to calculate the IC_{50} value by nonlinear regression. In this assay, papaverine was used as the reference compound. The enzymatic activities of the catalytic domain of other PDEs were measured with ^{3}H-cAMP or ^{3}H-cGMP as the substrate in similar protocols.

Crystallization and Structure Refinement

The crystals of PDE10A2 were grown by mean of using the hanging drop method and protocols similar to those previously reported.[31,45] Briefly, the unliganded PDE10A2 enzyme (10 mg/mL in a buffer composed of 20 mM Tris-HCl (pH = 7.5), 50 mM NaCl, 1 mM EDTA and 1 mM β-mercaptoethanol) was vapor-diffused against the well buffer of 0.1 M Hepes (pH = 7.5), 0.2 M $MgCl_2$, 18% PEG3350 and 50 mM 2-

mercaptoethanol. The complex of PDE10A2 with compound **1i** or **2b** was prepared by soaking the unliganded crystals in 10 mM solution of compound **1i** or **2b** in a buffer composed of 0.1 M Hepes (pH = 7.5), 0.1 M $MgCl_2$, 16% PEG 3350 and 60 mM 2-ME at 4 °C for 24 h. The crystallization buffer containing 20% ethylene glycol was used as the cryosolvent. Diffraction data were collected at 100 K on an in-house Oxford Diffraction Xcalibur Nova diffractometer. The data were processed using the program *CrysAlis Pro* and the structures were solved and refined using *CCP4* and *Phenix*.[46,47] The coordinates and structure factors have been deposited in the Protein Data Bank with PDB ID of 6kO0 and 6KO1, respectively. Data collection and refinement statistics for all structures were shown in supporting information.

Molecular Docking

The cocrystal structure of PDE10A with a potent and selective inhibitor (PDB ID: 3QPN) was used for molecular docking by the Surflex-dock method embedded in Tripos Sybyl X2.0.[48] The zinc and magnesium ions in the catalytic pocket were retained in the protein since they played important roles in the catalytic activity. Three water molecules coordinating the two ions were also retained. Particularly, the oxygen between the two ions was treated as a hydroxide ion according to previous report. His515, which was capable of donating a proton in catalytic reaction, was regarded as HIP (protonated histidine).[49] Hydrogen atoms were added according to amino acid templates and all ionizable residues were protonated at the neutral pH. Next, the protomol, which was representative of a set of molecular fragments characterizing the docking site, was generated in a ligand-based approach. All parameters for the protomol generation were set as default. The proto thresh and proto bloat were set to 0.5 and 0, respectively.

Once the protomol was well established, molecules were docked to PDE10A. For each molecule, 10 binding poses with the highest docking scores were obtained and each best pose with the appropriate binding pattern was retained for the following MD simulations.

Molecular Dynamics Simulation

Preparation of each ligand-PDE10 complex was as follows. First, partial atomic charges of the ligand were calculated by the Hartree-Fock method and 6-31G(d) basis set using Gaussian 03 program.[50] Then the restricted electrostatic potential (RESP) and general amber force field (GAFF) parameters were generated by antechamber program in Amber16.[51] Protein was assigned the amber03 force field, in addition that zinc and magnesium ions in the catalytic site were prepared using "nonbond model" method.[52] All amino acid residues have been well protonated in the molecular docking step. Since the whole system is neutral, no Na^+ or Cl^- was added. Finally, an 8 Å truncated octahedral water box of TIP3P model was added.

MD simulations were conducted by the following steps previously reported in our study.[53,54] First, each system was optimized by 4 steps of minimization with decreasing restrictions. Then, the whole system was heated gradually to 300K in 50 ps by the Langevin dynamics method in an *NVT* ensemble, followed by equilibration for 100 ps with a weak constraint of 10 kcal/(mol·Å^2) on heavy atoms of the protein in an *NPT* ensemble (p = 101kPa).[55] Finally, each system was subjected to 8 ns MD simulations under the periodic boundary conditions with an 8 Å cut-off for van der Waals interactions and partial mesh Ewald (PME) method for long-range electrostatic interactions.[56] The time step of MD simulations was assigned 2 fs. All bonds composed by hydrogens and heavy atoms were restricted by the SHAKE algorithm.[57] MM/GBSA binding free energies were calculated using the snapshots extracted from MD trajectories of the last 1 ns with 10 ps time interval.[33, 34]

Metabolic Stability in the rat liver microsomes

The assays of compounds **2b**, **3a** and **3c** were performed at the Medicilon Company, Shanghai, China. The experimental procedures were similar to those in our previous study. Compounds **2b**, **3a** and **3c** was dissolved in 100% DMSO to prepare a 0.5 mM stock solution and diluted to a final concentration of 1.5 μM for the experiments.

The assays of compounds **3d-3f** and **TAK-063** were performed as followed: microsomes in 0.1 M TRIS buffer pH 7.4 (final concentration 0.33 mg/mL), co-factor $MgCl_2$ (final concentration 5 mM) and tested compound (final concentration 0.1 μM, co-solvent (0.01% DMSO) and 0.005% Bovin serum albumin (BSA)) were incubated

at 37°C for 10 min. The reaction was started by the addition of NADPH (final concentration 1 mM). Aliquots were sampled at 0, 7, 17, 30 and 60 min respectively and methanol (cold in 4 °C) was added to terminate the reaction. After centrifugation (4000 rpm, 5 min), samples were then analyzed by LC-MS/MS.

ASSOCIATED CONTENT

Supporting Information

Diffraction data and structure refinement statistics; Characterization of target compounds; ^{1}H NMR, ^{13}C NMR, High-resolution mass spectra (HRMS) data; HPLC spectra data for tested compounds. This material is available free of charge *via* the Internet.

Accession Codes

The atomic coordinates and structure factors have been deposited into the RCSB Protein Data Bank with accession number 6KO0 and 6KO1. Authors will release the atomic coordinates and experimental data upon article publication.

■ AUTHOR INFORMATION

Corresponding Authors

* E-mail: guolei7@mail.sysu.edu.cn (L. Guo), wudeyan3@mail.sysu.edu.cn (D. Wu); Fax: +86-20-3994 3000

ORCID

Chen Zhang: 0000-0002-0447-0961
Yi-you Huang: 0000-0002-0712-1310
Yinuo Wu: 0000-0003-3071-5333
Lei Guo: 0000-0002-1905-1364
Deyan Wu: 0000-0001-5855-8662
Hai-Bin Luo: 0000-0002-2163-0509

Author Contributions

‖ These authors contributed equally to this work. D. Wu, L. Guo, and H.-B. Luo designed the research. Y.-F. Yu performed the synthetic work. C. Zhang and Z. Li performed molecular docking and dynamic simulation calculations. Y.-Y. Huang, S. Zhang, and Q. Zhou performed the biological tests. D. Wu, L. Guo, Y.-F. Yu, C. Zhang, Y.-Y. Huang, X. Li, Z. Lai, Y. Gao, Y. Wu, H.-B. Luo contributed to data analysis, writing, review, and revision of the manuscript.

Notes

The authors declare no competing financial interest.

ABBREVIATIONS USED

BINAP, (±)-2,2'-bis(diphenylphosphino)-1,1'-binaphthyl; cAMP, cyclic adenosine monophosphate; cGMP, cyclic guanosine monophosphate; CNS, central nervous system; DMF, N,N-dimethylformamide; DMSO, dimethyl sulfoxide; DIPEA, N,N-diisopropylethylamine; HATU, 2-(7-Azabenzotriazol-1-yl)-N,N,N',N'-tetrameth-yluroniumhexafluorophosphate; IC_{50}, half maximal inhibitory concentration; MD, molecular dynamics; PAH, pulmonary arterial hypertension; PDE, phosphodiesterase; PDE10, phosphodiesterase-10; SPBG, selective pocket binding group; TLC, thin layer chromatography; TMS, tetramethylsilane.

ACKNOWLEDGEMENTS

This work was supported by Natural Science Foundation of China (81872727, 81602955, 21702238, 21708052 and 81703341), Guangzhou Science and Technology Project (The People's Livelihood Programs for Science and Technology) (201803010075), Science Foundation of Guangdong Province (2016A030310144), The Fundamental Research Funds for the Central Universities (Sun Yat-Sen University) (No. 17ykjc03, 17ykpy20 and 19ykpy123), and Postdoctoral Science Foundation of China (2019M663326). We cordially thank Prof. H. Ke from Department of Biochemistry and Biophysics at the University of North Carolina, Chapel Hill, for his proofreading and his help with molecular cloning, expression, purification, crystal structure, and bioassay of PDEs.

REFERENCES

(1) Saha, S., Chant, D., Welham, J., and McGrath, J. (2005) A systematic review of the prevalence of schizophrenia. *PLoS Med. 2*, e141-e141.

(2) Van Os, J., and Kapur, S. (2009) Schizophrenia. *Lancet 374*, 635-645.

(3) Dervaux, A., and Laqueille, X. (2009) Mortality in patients with schizophrenia. *Lancet 374*, 1592.

(4) Newcomer, J. (2005) Second-generation (atypical) antipsychotics and metabolic effects. *CNS Drugs 19 Suppl 1*, 1-93.

(5) Yang, S.-W., Smotryski, J., McElroy, W. T., Tan, Z., Ho, G., Tulshian, D., Greenlee, W. J., Guzzi, M., Zhang, X., Mullins, D., Xiao, L., Hruza, A., Chan, T. M., Rindgen, D., Bleickardt, C., and Hodgson, R. Discovery of orally active

pyrazoloquinolines as potent PDE10 inhibitors for the management of schizophrenia. *Bioorg. Med. Chem. Lett. 22*, 235-239.

(6) Leucht, S., Corves, C., Arbter, D., Engel, R. R., Li, C., and Davis, J. M. (2009) Second-generation versus first-generation antipsychotic drugs for schizophrenia: a meta-analysis. *Lancet 373*, 31-41.

(7) Krogmann, A., Peters, L., von Hardenberg, L., Bodeker, K., Noles, V. B., and Correill, C. U. (2019) Keeping up with the therapeutic advances in schizophrenia: a review of novel and emerging pharmacological entities. *Cns Spectrums 24*, 41-68.

(8) Manallack, D. T., Hughes, R. A., and Thompson, P. E. (2005) The next generation of phosphodiesterase inhibitors: Structural clues to ligand and substrate selectivity of phosphodiesterases. *J. Med. Chem. 48*, 3449-3462.

(9) Bender, A. T., and Beavo, J. A. (2006) Cyclic nucleotide phosphodiesterases: molecular regulation to clinical use. *Pharmacol. Rev. 58*, 488.

(10) Conti, M., and Beavo, J. (2007) Biochemistry and physiology of cyclic nucleotide phosphodiesterases: essential components in cyclic nucleotide signaling. *Annu. Rev. Biochem. 76*, 481-511.

(11) Jeon, Y. H., Heo, Y. S., Kim, C. M., Hyun, Y. L., Lee, T. G., Ro, S., and Cho, J. M. (2005) Phosphodiesterase: overview of protein structures, potential therapeutic applications and recent progress in drug development. *Cell. Mol. Life Sci. 62*, 1198-1220.

(12) Arif, S. A., and Poon, H. (2011) Tadalafil: a long-acting phosphodiesterase-5 inhibitor for the treatment of pulmonary arterial hypertension. *Clin. Ther. 33*, 993-1004.

(13) Beavo, J. A. (1995) Cyclic nucleotide phosphodiesterases: functional implications of multiple isoforms. *Physiol. Rev. 75*, 725-748.

(14) Xie, Z., Adamowicz, W. O., Eldred, W. D., Jakowski, A. B., Kleiman, R. J., Morton, D. G., Stephenson, D. T., Strick, C. A., Williams, R. D., and Menniti, F. S. (2006) Cellular and subcellular localization of PDE10A, a striatum-enriched phosphodiesterase. *Neuroscience 139*, 597-607.

(15) Turetsky, B. I., and Moberg, P. J. (2009) An odor-specific threshold deficit implicates abnormal intracellular cyclic AMP signaling in schizophrenia. *Am. J. Psychiat. 166*, 226-233.

(16) Padovan-Neto, F. E., Sammut, S., Chakroborty, S., Dec, A. M., Threlfell, S., Campbell, P. W., Mudrakola, V., Harms, J. F., Schmidt, C. J., and West, A. R. (2015) Facilitation of corticostriatal transmission following pharmacological inhibition of striatal phosphodiesterase 10A: role of nitric oxide-soluble guanylyl cyclase-cGMP signaling pathways. *J. Neurosci. 35*, 5781-5791.

(17) Seeger, T. F., Bartlett, B., Coskran, T. M., Culp, J. S., James, L. C., Krull, D. L., Lanfear, J., Ryan, A. M., Schmidt, C. J., Strick, C. A., Varghese, A. H., Williams, R. D., Wylie, P. G., and Menniti, F. S. (2003) Immunohistochemical localization of PDE10A in the rat brain. *Brain Res. 985*, 113-126.

(18) Lakics, V., Karran, E. H., and Boess, F. G. (2010) Quantitative comparison of phosphodiesterase mRNA distribution in human brain and peripheral tissues. *Neuropharmacology 59*, 367-374.

(19) Hebb, A. L. O., and Robertson, H. A. (2007) Role of phosphodiesterases in

neurological and psychiatric disease. *Curr. Opin. Pharm. 7*, 86-92.

(20) Chappie, T. A., Helal, C. J., and Hou, X. (2012) Current landscape of phosphodiesterase 10A (PDE10A) inhibition. *J. Med. Chem. 55*, 7299-7331.

(21) Siuciak, J. A., McCarthy, S. A., Chapin, D. S., Fujiwara, R. A., James, L. C., Williams, R. D., Stock, J. L., McNeish, J. D., Strick, C. A., Menniti, F. S., and Schmidt, C. J. (2006) Genetic deletion of the striatum-enriched phosphodiesterase PDE10A: Evidence for altered striatal function. *Neuropharmacology 51*, 374-385.

(22) Siuciak, J. A., Chapin, D. S., Harms, J. F., Lebel, L. A., McCarthy, S. A., Chambers, L., Shrikhande, A., Wong, S., Menniti, F. S., and Schmidt, C. J. (2006) Inhibition of the striatum-enriched phosphodiesterase PDE10A: A novel approach to the treatment of psychosis. *Neuropharmacology 51*, 386-396.

(23) Kehler, J. (2013) Phosphodiesterase 10A inhibitors: a 2009-2012 patent update. *Expert Opin. Ther. Pat. 23*, 31-45.

(24) Bartolome-Nebreda, J. M., Conde-Ceide, S., and Garcia, M. (2015) Phosphodiesterase 10A inhibitors: analysis of US/EP patents granted since 2012. *Pharmaceutical Patent Analyst 4*, 161-186.

(25) Zagórska, A. (2019) Phosphodiesterase 10 (PDE10) inhibitors: an updated patent review (2014-present), Expert Opinion on Therapeutic Patents. *Expert Opin. Ther. Pat. 30*, 147-157.

(26) Barret O, Thomae D, Tavares A, Alagille, D., Papin, C., Waterhouse, R., McCarthy, T., Jennings, D., Marek, K., Russell, D., Seibyl, J., and Tamagnan, G. In Vivo Assessment and Dosimetry of 2 novel PDE10A PET radiotracers in humans: F-18-MNI-659 and F-18-MNI-654. *J Nucl Med. 55*, 1297-1304.

(27) Toth M, Haggkvist J, Stepanov V., Takano, A., Nakao, R., Amini, N., Miura, S., Kimura, H., Taniguchi, T., Gulyas, B., and Halldin, C. (2015) Molecular imaging of PDE10A knockout mice with a novel PET radiotracer: [C-11]T-773. *Mol Imaging Biol. 17*,445-449.

(28) Geerts H, Spiros A, Roberts P. (2017) Phosphodiesterase 10 inhibitors in clinical development for CNS disorders. *Expert Rev Neurother. 17*, 553-560.

(29) Macek, T. A., McCue, M., Dong, X., Hanson, E., Goldsmith, P., Affinito, J., and Mahableshwarkar, A. R. (2019) A phase 2, randomized, placebo-controlled study of the efficacy and safety of TAK-063 in subjects with an acute exacerbation of schizophrenia. *Schizophr. Res. 204*, 289-294.

(30) Card, G. L., England, B. P., Suzuki, Y., Fong, D., Powell, B., Lee, B., Luu, C., Tabrizizad, M., Gillette, S., Ibrahim, P. N., Artis, D. R., Bollag, G., Milburn, M. V., Kim, S. H., Schlessinger, J., and Zhang, K. Y. J. (2004) Structural basis for the activity of drugs that inhibit phosphodiesterases. *Structure 12*, 2233-2247.

(31) Huang, Y.-Y., Yu, Y.-F., Zhang, C., Chen, Y., Zhou, Q., Li, Z., Zhou, S., Li, Z., Guo, L., Wu, D. Y., Wu, Y. N., and Luo, H. B. (2019) Validation of phosphodiesterase-10 as a novel target for pulmonary arterial hypertension via highly selective and subnanomolar inhibitors. *J. Med. Chem. 62*, 3707-3721.

(32) Shipe, W. D., Sharik, S. S., Barrow, J. C., McGaughey, G. B., Theberge, C. R., Uslaner, J. M., Yan, Y., Renger, J. J., Smith, S. M., Coleman, P. J., and Cox, C. D. (2015) Discovery and optimization of a series of pyrimidine-based phosphodiesterase

10A (PDE10A) inhibitors through fragment screening, structure-based design, and parallel synthesis. *J. Med. Chem. 58*, 7888-7894.

(33) Hou, T., Wang, J., Li, Y., and Wang, W. (2011) Assessing the performance of the MM/PBSA and MM/GBSA methods. 1. The accuracy of binding free energy calculations based on molecular dynamics simulations. *J. Chem. Inf. Model. 51*, 69-82.

(34) Massova, I., and Kollman, P. A. (2000) Combined molecular mechanical and continuum solvent approach (MM-PBSA/GBSA) to predict ligand binding. *Perspect. Drug Discov. Des. 18*, 113-135.

(35) Helguera, A. M., Pérez-Garrido, A., Gaspar, A., Reis, J., Cagide, F., Vina, D., Cordeiro, M. N. D. S., and Borges, F. (2013) Combining QSAR classification models for predictive modeling of human monoamine oxidase inhibitors. *Eur. J. Med. Chem. 59*, 75-90.

(36) Ye, X., Moeljadi, A. M. P., Chin, K. F., Hirao, H., Zong, L., and Tan, C.-H. (2016) Enantioselective sulfoxidation catalyzed by a bisguanidinium diphosphatobisperoxotungstate ion pair. *Angew. Chem. 13*, 7101-7105.

(37) Mukhina, O. A., Kuznetsov, D. M., Cowger, T. M., and Kutateladze, A. G. (2015) Amino azaxylylenes photogenerated from o-Amido imines: photoassisted access to complex Spiro-Poly-Heterocycles. *Angew. Chem. 54*, 11516-11520.

(38) Chino, A., Masuda, N., Amano, Y., Honbou, K., Mihara, T., Yamazaki, M., and Tomishima, M. (2014) Novel benzimidazole derivatives as phosphodiesterase 10A (PDE10A) inhibitors with improved metabolic stability. *Biorg. Med. Chem. 22*, 3515-3526.

(39) Thanigaimalai, P., Le Hoang, T. A., Lee, K.-C., Sharma, V. K., Bang, S.-C., Yun, J. H., Roh, E., Kim, Y., and Jung, S.-H. (2010) Synthesis and evaluation of novel chromone analogs for their inhibitory activity against interleukin-5. *Eur. J. Med. Chem. 45*, 2531-2536.

(40) Breslin, H. J., Diamond, C. J., Kavash, R. W., Cai, C., Dyatkin, A. B., Miskowski, T. A., Zhang, S.-P., Wade, P. R., Hornby, P. J., and He, W. (2012) Identification of a dual δ OR antagonist/μ OR agonist as a potential therapeutic for diarrhea-predominant Irritable Bowel Syndrome (IBS-d). *Bioorg. Med. Chem. Lett. 22*, 4869-4872.

(41) Ren, J., He, Y., Chen, W. Y., Chen, T. T., Wang, G., Wang, Z., Xu, Z. J., Luo, X. M., Zhu, W. L., Jiang, H. L., Shen, J. S., and Xu, Y. C. (2014) Thermodynamic and structural characterization of halogen bonding in protein–ligand interactions: a case study of PDE5 and its inhibitors. *J. Med. Chem. 57*, 3588-3593.

(42) Reis, J., Cagide, F., Chavarria, D., Silva, T., Fernandes, C., Gaspar, A., Uriarte, E., Remião, F., Alcaro, S., Ortuso, F., and Borges, F. (2016) Discovery of new chemical entities for old targets: insights on the lead optimization of chromone-based Monoamine Oxidase B (MAO-B) inhibitors. *J. Med. Chem. 59*, 5879-5893.

(43) Mori, K., Murase, T., and Fujita, M. (2015) One-step synthesis of [16]Helicene. *Angew. Chem. Int. Ed. 54*, 6847-6851.

(44) Huang, Y., Liu, X., Wu, D., Tang, G., Lai, Z., Zheng, X., Yin, S., and Luo, H.-B. (2017) The discovery, complex crystal structure, and recognition mechanism of a novel natural PDE4 inhibitor from Selaginella pulvinata. *Biochem. Pharmacol. 130*, 51-59.

(45) Wang, H., Liu, Y., Hou, J., Zheng, M., Robinson, H., and Ke, H. (2007) Structural

insight into substrate specificity of phosphodiesterase 10. *Proc. Natl. Acad. Sci. U. S. A. 104*, 5782-5787.

(46) Adams, P. D., Afonine, P. V., Bunkóczi, G., Chen, V. B., Davis, I. W., Echols, N., Headd, J. J., Hung, L.-W., Kapral, G. J., Grosse-Kunstleve, R. W., McCoy, A. J., Moriarty, N. W., Oeffner, R., Read, R. J., Richardson, D. C., Richardson, J. S., Terwilliger, T. C., and Zwart, P. H. (2010) PHENIX: a comprehensive Python-based system for macromolecular structure solution. *Acta Crystallogr. D Biol. Crystallogr. 66*, 213-221.

(47) Winn, M. D., Ballard, C. C., Cowtan, K. D., Dodson, E. J., Emsley, P., Evans, P. R., Keegan, R. M., Krissinel, E. B., Leslie, A. G. W., McCoy, A., McNicholas, S. J., Murshudov, G. N., Pannu, N. S., Potterton, E. A., Powell, H. R., Read, R. J., Vagin, A., and Wilson, K. S. (2011) Overview of the CCP4 suite and current developments. *Acta Crystallogr. D Biol. Crystallogr. 67*, 235-242.

(48) Jain, A. N. (2003) Surflex: fully automatic flexible molecular docking using a molecular similarity-based search engine. *J. Med. Chem. 46*, 499-511.

(49) Li, Z., Wu, Y., Feng, L.-J., Wu, R., and Luo, H.-B. (2014) Ab initio QM/MM study shows a highly dissociated SN2 hydrolysis mechanism for the cGMP-specific phosphodiesterase-5. *J. Chem. Theory Comput. 10*, 5448-5457.

(50) Frisch, M. J., Trucks, G. W., Schlegel, H. B., Scuseria, G. E., Robb, M. A., Cheeseman, J. R., Montgomery, J. A., Vreven, T., Kudin, K. N., Burant, J. C., Millam, J. M., Iyengar, S. S., Tomasi, J., Barone, V., Mennucci, B., Cossi, M., Scalmani, G., Rega, N., Petersson, G. A., Nakatsuji, H., Hada, M., Ehara, M., Toyota, K., Fukuda, R., Hasegawa, J., Ishida, M., Nakajima, T., Honda, Y., Kitao, O., Nakai, O., Klene, M., Li, X., Knox, J. E., Hratchian, H. P., Cross, J. B., Bakken, V., Adamo, C., Jaramillo, J., Gomperts, R., Stratmann, R. E., Yazyev, O., Austin, A. J., Cammi, R., Pomelli, C., Ochterski, J. W., Ayala, P. Y., Morokuma, K., Voth, G. A., Salvador, P., Dannenberg, J. J., Zakrzewski, V. G., Dapprich, S., Daniels, A. D., Strain, M. C., Farkas, O., Malick, D. K., Rabuck, A. D., Raghavachari, K., Foresman, J. B., Ortiz, J. V., Cui, Q., Baboul, A. G., Clifford, S., Cioslowski, J., Stefanov, B. B., Liu, G., Liashenko, A., Piskorz, P., Komaromi, I., Martin, R. L., Fox, D. J., Keith, T., Al-Laham, M. A., Peng, C. Y., Nanayakkara, A., Challacombe, M., Gill, P. M. W., Johnson, B., Chen, W., Wong, M. W., Gonzalez, C., and Pople, J. A. *Gaussian 03*, Revision E.01; Gaussian, Inc.: Pittsburgh PA, 2004.

(51) Wang, J., Wang, W., Kollman, P. A., and Case, D. A. (2006) Automatic atom type and bond type perception in molecular mechanical calculations. *J. Mol. Graphics Model. 25*, 247-260.

(52) Stote, R. H., and Karplus, M. (1995) Zinc binding in proteins and solution: A simple but accurate nonbonded representation. *Proteins 23*, 12-31.

(53) Li, Z., Cai, Y.-H., Cheng, Y.-K., Lu, X., Shao, Y.-X., Li, X., Liu, M., Liu, P., and Luo, H.-B. (2013) Identification of novel phosphodiesterase-4D inhibitors prescreened by molecular dynamics-augmented modeling and validated by bioassay. *J. Chem. Inf. Model. 53*, 972-981.

(54) Zhang, C., Feng, L.-J., Huang, Y., Wu, D., Li, Z., Zhou, Q., Wu, Y., and Luo, H.-B. (2017) Discovery of novel phosphodiesterase-2A inhibitors by structure-based

virtual screening, structural optimization, and bioassay. *J. Chem. Inf. Model. 57*, 355-364.

(55) Schlick, T. Molecular Dynamics: Basics. Molecular Modeling and Simulation, 1; Bloch, A., Epstein, C.L., etc., Eds.; Interdisciplinary Applied Mathematics; *Springer-Verlag: New York*, 2002; 21, 383-418.

(56) Salomon-Ferrer, R., Götz, A. W., Poole, D., Le Grand, S., and Walker, R. C. (2013) Routine microsecond molecular dynamics simulations with AMBER on GPUs. 2. explicit solvent particle mesh ewald. *J. Chem. Theory Comput. 9*, 3878-3888.

(57) R. Forester, T., and Smith, W. (2000) SHAKE, rattle, and roll: Efficient constraint algorithms for linked rigid bodies. *J. Comput. Chem. 19*, 102-111.

For Table of Contents Use Only

Discovery and Optimization of Chromone Derivatives as Novel Selective Phosphodiesterase 10 Inhibitors

Yan-Fa Yu[||], Chen Zhang[||], Yi-You Huang[||], Sirui Zhang, Qian Zhou, Xiangmin Li, Zengwei Lai, Zhe Li, Yuqi Gao, Yinuo Wu, Lei Guo*, Deyan Wu*, and Hai-Bin Luo

School of Pharmaceutical Sciences, Sun Yat-sen University, Guangzhou 510006, China